Ore Geology Reviews 73 (2016) 179–197

Contents lists available at ScienceDirect

Ore Geology Reviews

journal homepage: www.elsevier.com/locate/oregeorev

The Gaosongshan epithermal gold deposit in the Lesser Hinggan Range of the Heilongjiang Province, NE China: Implications for Early Cretaceous mineralization

Baiwu Hao [a,b,*], Jun Deng [b], Leon Bagas [c,d], Liangsheng Ge [a], Fengjun Nie [d], Susan Turner [e], Min Qing [a]

[a] Gold Geology Institute of the Chinese Armed Police Force, Langfang 065000, China
[b] State Key Laboratory of Geological Processes and Mineral Resource, China University of Geosciences, Beijing 100083, China
[c] Centre for Exploration Targeting, The University of Western Australia, Crawley, WA 6009, Australia
[d] Institute of Mineral Deposits, Chinese Academy of Geological Sciences, Beijing 100037, China
[e] Queensland Museum, Geology/Palaeontology, 122 Gerler Road, Hendra, Queensland 4101, Australia

ARTICLE INFO

Article history:
Received 21 February 2015
Received in revised form 13 March 2015
Accepted 16 March 2015
Available online 18 March 2015

Keywords:
Gaosongshan
Epithermal gold
Gold precipitation
Source of mineralization
Geochronology
Lesser Hinggan Range
NE China

ABSTRACT

The newly discovered and large ca. 99 Ma Gaosongshan gold deposit is located in the Lesser Hinggan (or Xinggan) Range to the west of the Jiamusi Massif. The deposit is located at the border of the Great Hinggan Range–Mongolian Orogen with the Circum-Pacific tectonic belt and has a resource of ~22 t @ 6.3 g/t Au. Gaosongshan is classified as an adularia–sericite epithermal deposit associated with the large tensional Shaqihe Fault and has a low-sulfide content with a high concentration of gold hosted by pure chalcedonic quartz, which makes the deposit both unique and economically important in the area. Early Cretaceous volcanic rocks host the deposit as well as other gold deposits in the region. The mineralization at Gaosongshan includes Au, Ag, Mo, Sb, As, Pb and Hg. Stable isotope studies of fluid inclusions associated with the mineralization suggest that the mineralizing fluid had a meteoric origin ($D_{V\text{-}SMOW}$: −129 to −111‰; $^{18}O_{fluid}$: 7.9 to 13.8‰). Fluid inclusion thermography indicates that the mineralized fluid was between 150° and 310 °C and had a low salinity (0.7–3.71 wt.% NaCl), low density (0.48–0.94 g/cm^3), shallow metallogenic depth (430–1270 m), and a large amount of reducing gaseous components (CH_4, C_2H_6, CO, N_2, and CO_2). The presence of large quantities of flaky quartz, adularia, gas-rich fluid inclusions, low-sulfide minerals and pure gold-bearing chalcedonic quartz suggests that fluid boiling was the principal mechanism for the gold precipitation. Sulfur isotopic data ($\delta^{34}S$: ~ −2.4 to 2.9‰) indicate a deep magmatic origin for the mineralization, and the Pb isotopes ($^{206}Pb/^{204}Pb$: 18.14–18.46; $^{207}Pb/^{204}Pb$: 15.51–15.57; $^{208}Pb/^{204}Pb$: 38.01–38.40) also indicate that the metallogenic source of the deposit contained a significant mantle component. The mineralizing fluid interacted with a Late Paleozoic (ca. 260–253 Ma) substrate and ca. 141–91 Ma volcanic host rocks. The geological and geochemical characteristics of the deposit, and the Tuanjiegou, Dongan, Sandaowanzi and other large gold deposits represent an Early Cretaceous (114–80 Ma) epithermal mineralizing events in the Lesser Hinggan Range. The belt is controlled by the volcanic Sunwu–Jiayin Basin formed in a back-arc extensional setting along an active continental margin in East China, and the gold deposits in the belt have the same genesis as porphyritic Au(–Cu) deposits along the continental margin in eastern Jilin and Heilongjiang provinces. It is here proposed that the mineralization in both regions is related to the subduction of the Paleo-Pacific plate.

1. Introduction

Epithermal deposits are formed from circulating mineralized meteoric fluids or a mixture of meteoric and magmatic fluids driven by magma. This type of deposit generally forms at shallow depths in the crust and commonly contains precious, base metals, hydrargyrum, stibnite, alunite, and other non-metallic deposits deposited at pressures of <100 bars and temperatures of ~200–300 °C corresponding to depths of <2 km (e.g. Lindgren, 1922, 1933; Simmons et al., 2005). Hedenquist et al. (2000), Einaudi et al. (2003) and Sillitoe and Hedenquist (2003) classify such deposits as the high-sulfidation (alunite–kaolinite) type. These include Au–Ag–Cu deposits with vuggy quartz alteration, as well as with pyrophyllite–sericite alteration. The low-sulfidation (adularia–sericite) type of epithermal deposits commonly includes Au–Ag, and the intermediate-sulfidation type is characterized by base metals containing Sn–Ag or Ag–Au.

The common tectonic setting for low- and high-sulfidation epithermal types of Au deposits include island-arc, arcs along continental margins, back-arc extensional and fracturing zones developed in the hanging

* Corresponding author at: Gold Geology Institute of the Chinese Armed Police Force, Langfang 065000, China.

http://dx.doi.org/10.1016/j.oregeorev.2015.03.009
0169-1368/

wall of subduction zones (Sillitoe, 2000; Hedenquist et al., 2000; Corbett, 2002). Modern examples are present in the Circum-Pacific, Mediterranean–Himalaya orogen, and the Mongolia–Okhotsk Belt (Chen et al., 2001).

Many large (≥20 t), medium (5–20 t) and small (≤5 t) epithermal gold deposits have been discovered in the Lesser Hinggan Range, such as at Dong'an with a resource of 24.3 t @ 5.04 g/t Au (Guo et al., 2004; Z.C. Zhang et al., 2010), Tuanjiegou with a resource of 81.6 t@ 4.61 g/t Au (Li and Wang, 1998; Wang et al., 2004, 2012; Sun et al., 2008; Li et al., 2008; Xu et al., 2012), Sandaowan with a resource of >15 t @ 8.03 g/t Au (Liu et al., 2011; Han et al., 2011; Xu et al., 2012; Zhai et al., 2013), and Gaosongshan with a resource of ~22 t @ 6.3 g/t Au (documented below). As such, the region is considered very prospective for mineralization and is a popular region of studying gold deposits in China.

The newly discovered large Gaosongshan gold deposit is located in the Wuyi Range west of the Jiamusi Massif in the Heilongjiang Province of China, between the Great Hinggan Range in the Central Asian Orogen and Circum-Pacific Tectonic Belt (Fig. 1). The deposit is poorly understood, even though there are discussions on its geological characteristics and genesis in the literature (Liu et al., 2006; Bian et al., 2009; Tang et al., 2010). Specifically, the deposit's age and geological relationship with other gold deposits in the region is still not known.

It is observed in this contribution that the epithermal gold deposits in the Lesser Hinggan Range have the following common characteristics: (1) they are all Early Cretaceous (114–80 Ma) in age; (2) most of the deposits are hosted by Early Cretaceous volcanic rocks deposited in the fault-controlled Mesozoic Sunwu–Jiayin Basin; (3) the deposits commonly hosted by NW-trending faults; and (4) the deposits are in a back-arc extensional tectonic setting with faulting controlled by an active continental margin to the west of the Jiamusi Massif, which is associated with the subduction of the Mesozoic Izanagi plate beneath the Euro-Asian plate in eastern China. In addition, this contribution documents a better understanding of large-scale mineralization in the Mesozoic active continental margin associated with Circum-Pacific metallogenetic regions in eastern China.

2. Regional geology

The Lesser Hinggan Range is located in the Yichun–Yanshou Fold Zone between the Songnen and Jiamusi–Xingkai massifs (Wilde et al., 2010; Zhou et al., 2010). The range has developed in the faulted Mesozoic volcanic Sunwu–Jiayin (Amur–Zeya) Basin that is controlled by NW-trending faults and subparallel magmatic belts.

The gold mineralization in the Lesser Hinggan Range is situated to the west of polymetallic (Fe–Mo–Pb–Zn–Au) mineralized zones and to

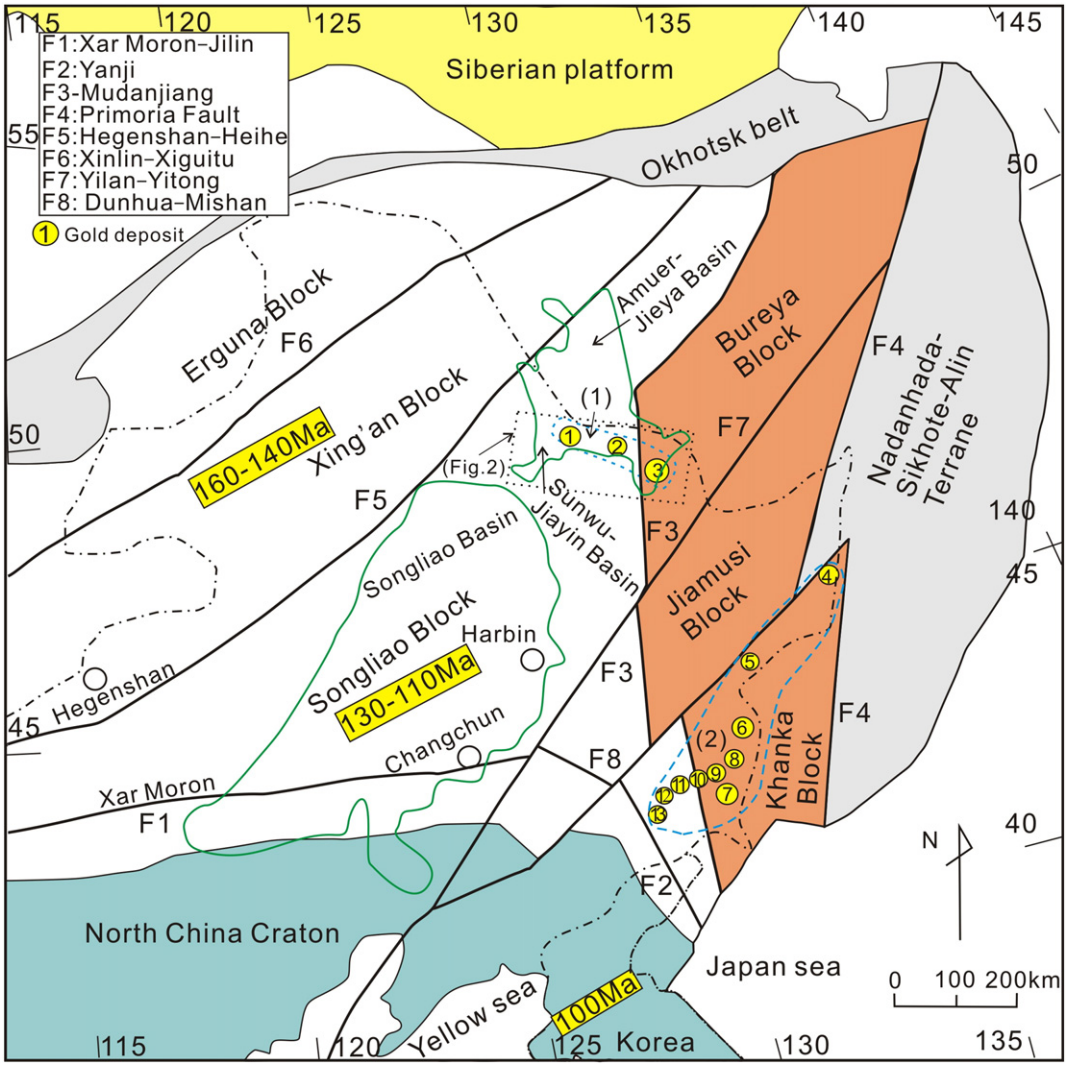

Fig. 1. Simplified tectonic map of NE China (modified after Zhou et al., 2009a, 2010). The eastward younging of igneous rocks from the Great Xinggan Range to southwestern Japan suggests an eastward migration of magmatism. (1) Lesser Xinggan Range gold belt, 1—Dongan; 2—Gaosongshan; 3—Tuangjiegou; and (2) Yanbian and Dongning Au(–Cu) mineralized belts including 4—Sipingshan, 5—Sishanlinchang, 6—Jinchang, 7—Xiaoxinancha, 8—Jiufogou, 9—Duhuangling, 10—Jiusangou, 11—Ciweigou, 12—Naozhi, 13—Wuxingshan and 14—Wufengshan.

the west of Jiamusi Massif in the Zhangguangcai and Lesser Hinggan ranges. Gold deposits in the region include those at Dong'an, Gaosongshan, Tuanjiegou, and Sandaowanzi in the most westerly Heihe area (Fig. 2, Liang et al., 2012; Fig. 3a, Bian et al., 2009).

2.1. Stratigraphy

The stratigraphy of the Zhangguangcai and Lesser Hinggan ranges is graphically summarized in Fig. 3a. Pre-Mesozoic (>210 Ma) rocks are commonly located in Paleo-Asian orogens between the Sino-Korean and Siberia cratons, and Mesozoic (<210 Ma) units are concentrated further to the east in the Circum-Pacific orogens affected by the subduction of the Paleo-Pacific plate (Xiao et al., 2003; Zhou et al., 2009a; Hao, 2012; Hao and Hou, 2012; Wu et al., 2011).

The rocks exposed in the Lesser Hinggan Range are Proterozoic to Neogene in age and the oldest units in the study are Proterozoic rocks in and around the Jurassic Jiamusi (Bureya) Massif (Fig. 3a; Zhou et al., 2009a). The Proterozoic Heilongjiang Complex (Pt_{2-3} h) forms a metamorphic crystalline complex consisting of orthogneiss, two-mica schist, muscovite–albite schist, marble, mafic schist and ultramafic rocks, which are metamorphosed at greenschist to blueschist facies. The group is in the Jiamusi Massif and at the intersection between the Zhangguangcai Range Massif and Songnen Block (Zhou et al., 2009a; Wilde et al., 2010). On passing, the presence of greenschist facies Late Triassic (224–213 Ma) basalt in the complex supports the suggestion that the area represents an accretion complex formed during the collision of the Songnen Block and Zhangguangcai Range Massif with the Jiamusi and Xingkai massifs.

Cambrian to Permian units unconformably overlie the Proterozoic crystalline units in the study area, and are predominantly shallow marine and marine sedimentary rocks at the base overlain by lacustrine–fluvial facies sandstone, siltstone, marble, and slate (Z.C. Zhang et al., 2010).

The location of the Early Paleozoic (ca. 545–540 Ma) magmatic rocks in the region are controlled by structures that were active along the margin of the Proterozoic continental margin (Sun et al., 2005; Liu et al., 2008). Also present are Late Paleozoic, and Late Paleozoic to Early Mesozoic granites forming batholiths and stocks distributed across large areas along the Tangwang River (Fig. 3a).

Jurassic–Cretaceous epicontinental clastic rocks and mafic to felsic volcanic rocks are closely associated with gold mineralization, and are assigned to the Banzifang (K_1b), Ningyuancun (K_1n), Yongqing (K_1y), Ganhe (K_{1g}) and Fuminhe (K_2f) formations (Zhao et al., 2011; Hao, 2013). Mesozoic volcanic rocks crop out to the west of the Jiamusi Massif on the southern side of the Wuyun and Jiayin basins (Figs. 2 and 3a; Liang et al., 2012).

Paleocene–Oligocene units form cap rocks in the region and consist of continental clastic rocks, and Quaternary sandstone, conglomerate and alkaline basalt are deposited in valleys (Z.C. Zhang et al., 2010).

2.2. Tectonic setting

Northeastern China has experienced complicated tectonic processes since the Paleozoic, including amalgamation, accretion and suturing among multiple terranes (Wu et al., 2011). During this period the Early Paleozoic Xinggan Block was accreted onto the ca. 490 Ma Erguna Block, the Songliao Block joined the Xinggan–Erguna Block, and the Liaoyuan Block joined the North China Craton (NCC). This was followed by the collision of the NCC and the Siberia Craton to the north during ca. 250 Ma forming the Central Asian Orogen (Wu et al., 2011). The Paleozoic and Mesozoic tectonic evolution of NE China ended with the closure of the Mesozoic (ca. 170–165 Ma) Okhotsk Ocean (Xu et al., 2013). By this period, the Jiamusi–Khanka Massif (Bureya Massif) and the Songnen Block had amalgamated, and the Heilongjiang and Raohe complexes were accreted onto the Nadanhada and Sikhote–Alin blocks (Zhou et al., 2009a, 2010; Wilde et al., 2010; Wu et al., 2011).

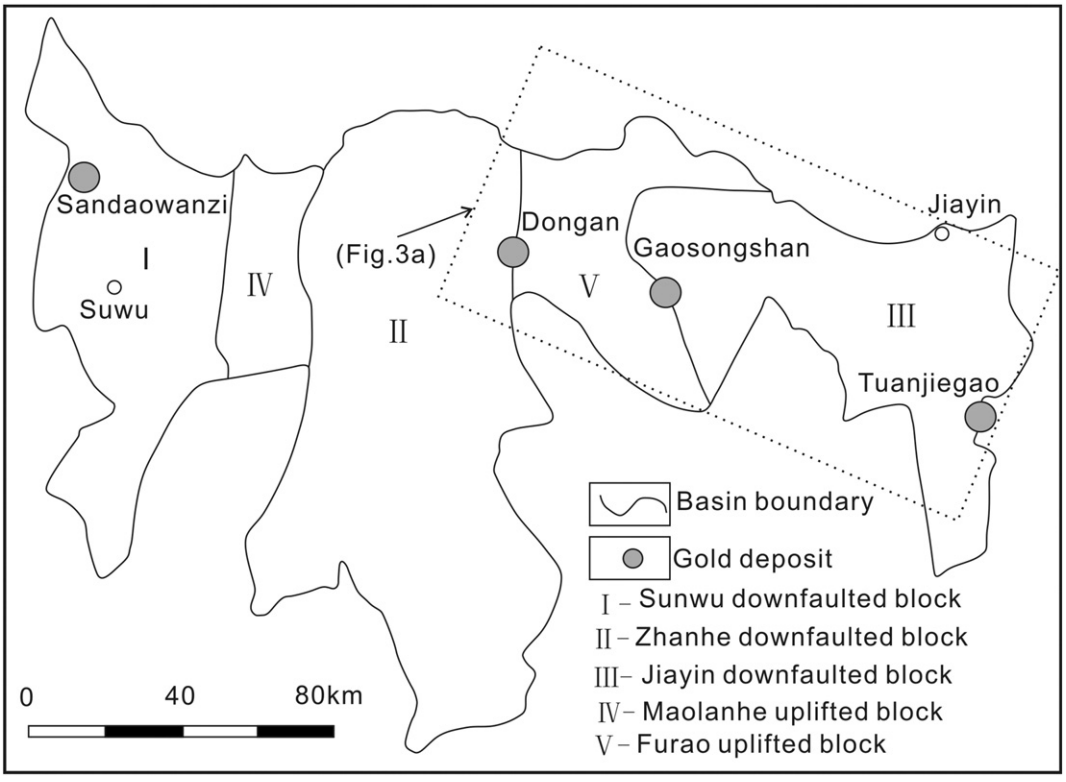

Fig. 2. Geological sketch of the fault-bound Sunwu and Jiayin volcanic basins (after Liang et al., 2012). The gold mineralization is concentrated along the edge of the NW-trending Lesser Xinggan Range.

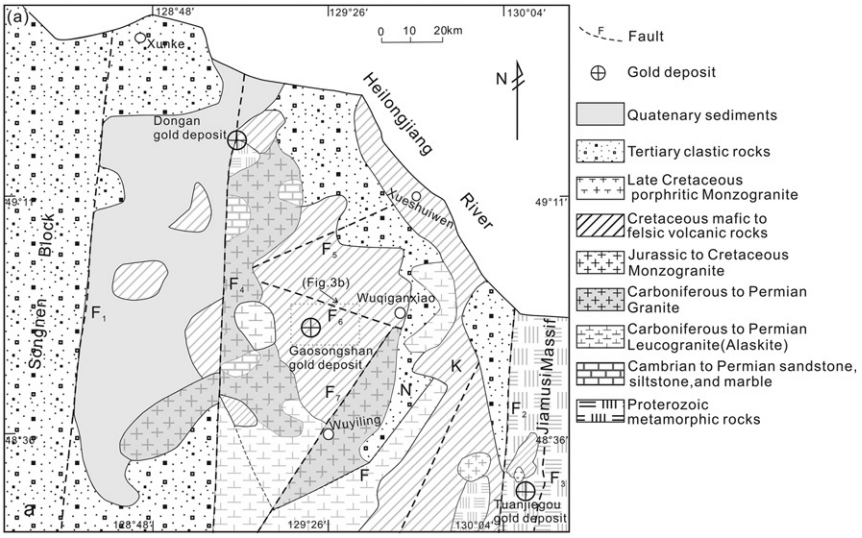
(a)
128°48′
129°26′
130°04′
0 10 20km
N
Xunke
Dongan gold deposit
Heilongjiang River
Xueshuiwen
49°11′
Songnen Block
F1
F2
F3
F4
F5
F6
F7
(Fig.3b)
Wuqiganxiao
Gaosongshan gold deposit
Wuyiling
K
N
Jiamusi Massif
48°36′
Tuanjiegou gold deposit
Fault
Gold deposit
Quatenary sediments
Tertiary clastic rocks
Late Cretaceous porphritic Monzogranite
Cretaceous mafic to felsic volcanic rocks
Jurassic to Cretaceous Monzogranite
Carboniferous to Permian Granite
Carboniferous to Permian Leucogranite(Alaskite)
Cambrian to Permian sandstone, siltstone,and marble
Proterozoic metamorphic rocks

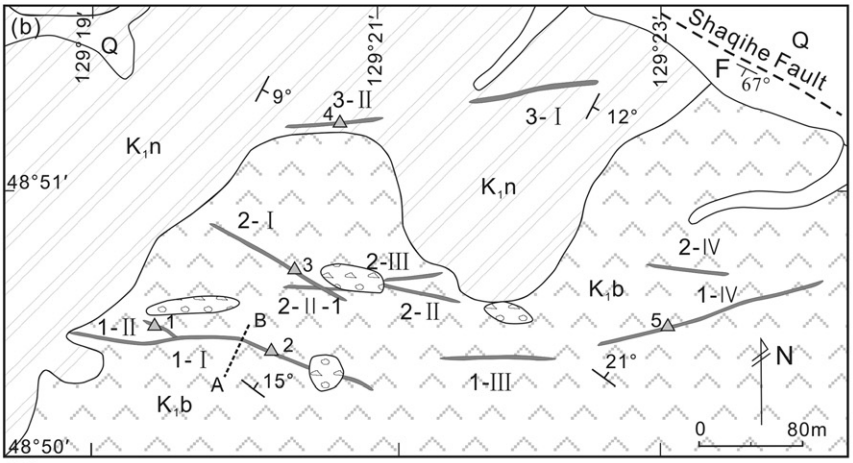
(b)
129°19′
Q
129°21′
129°23′
Shaqihe Fault
F 67°
9°
3-II
4
3-I
12°
K1n
48°51′
2-I
3
2-III
2-II-1
2-II
2-IV
K1b
1-IV
1-II
1
B
2
1-I
A
15°
5
21°
N
1-III
0 80m
48°50′

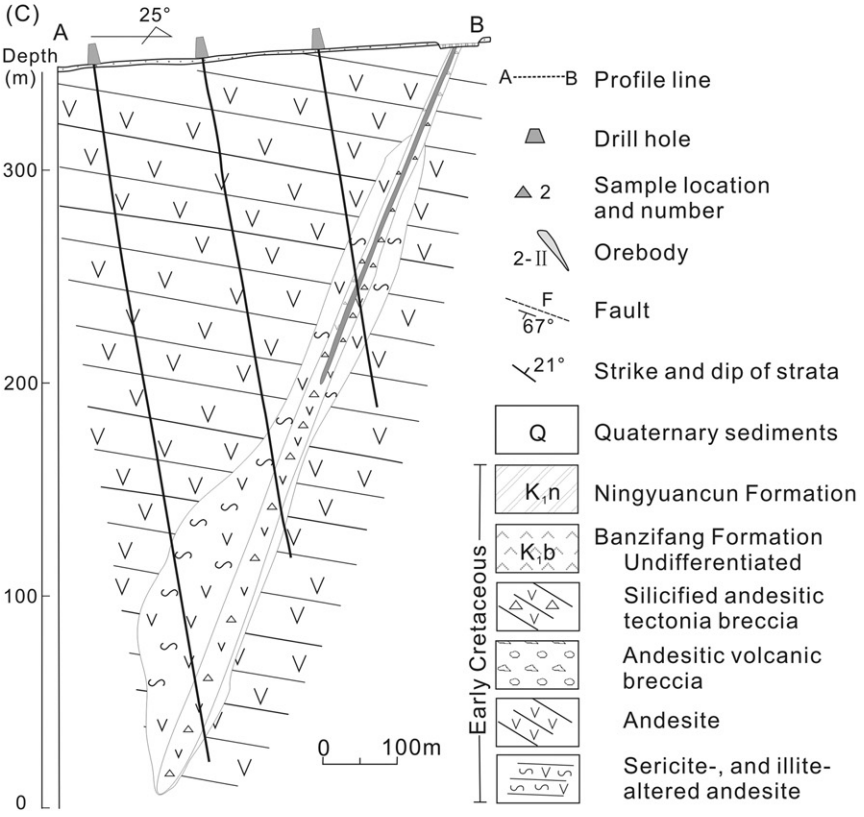
(C)
A
25°
B
Depth (m)
300
200
100
0
0 100m
A B Profile line
Drill hole
2 Sample location and number
2-II Orebody
F 67° Fault
21° Strike and dip of strata
Q Quaternary sediments
K1n Ningyuancun Formation
K1b Banzifang Formation Undifferentiated
Silicified andesitic tectonia breccia
Andesitic volcanic breccia
Andesite
Sericite-, and illite-altered andesite
Early Cretaceous

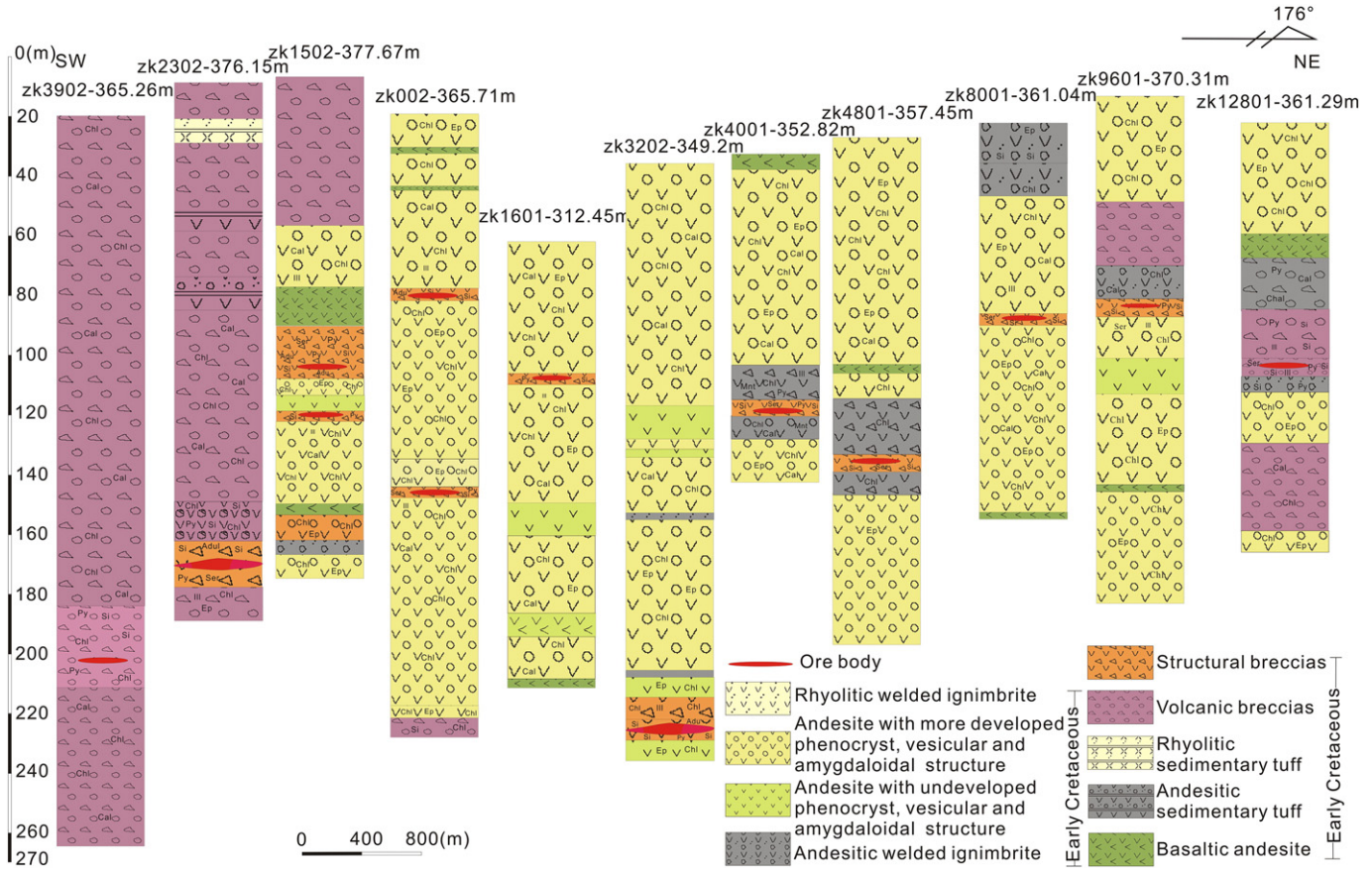

Fig. 4. Simplified geological sections of diamond-drill holes in the No. 1-I Vein at the Gaosongshan gold deposit. Alteration bordering the gold mineralization is marked by Si (silica)–Adu (adularia)–Ser (sericite) in the inner zone, Ser–Ill (illite)–Mnt (montmorillonite)–Chl (chlorite) in the intermediate zone, and Chl–Ep (epidote)–Cal (carbonate) in the outer zone.

The Mesozoic tectonic activities in the Mudanjiang Ocean, now represented by the Zhangguangcai and Lesser Hinggan ranges, included subduction followed by collision (Hao, 2013; Xu et al., 2013). In this period (specifically between ca. 200 and 170 Ma), polymetallic ore including Fe, Mo, Pb and Zn was deposited, including the Xiaoxilin Pb, and the Luming, Huojihe and Cuiling Mo deposits (Chen et al., 2012). This was followed by the deposition of epithermal gold deposits during 125–80 Ma, which are hosted by NW-trending faults and subparallel magmatic belts related to the late subduction of the Paleo-Pacific plate (Zhou et al., 2009b; Z.C. Zhang et al., 2010; Xu et al., 2013).

Fault-bound volcanic basins and faults are present in the study area, which includes early NE-, eastward- and WNW-trending faults developed below the basins (Liang et al., 2012). The NE-trending faults are extensional structures that control the development of the Songliao, and Sunwu–Jiayin basins, and are also associated with N-trending shearing faults such as the Wulaga, Mudanjiang and Kuerbin River faults. Eastward-trending faults such as the Heilongjiang and Xunhe faults located near the northern edge of the Sunwu–Jiayin Basin are strike-slip faults that are intersected by WNW-trending faults and shear zones. The WNW-trending structures are particularly important, because they host gold deposits such as at Gaosongshan in the Shaqihe Fault, and the Taxi–Linkou Fault that forms a boundary of the Lesser Hinggan Range and the Songliao Basin. These structures are strike-slip faults formed during simple shearing and form conjugate sets with the NE-trending faults. Also present are ENE-trending strike-slip faults that are subordinate to the WNW-trending faults and also host mineralization at Gaosongsha. The NW-trending faults at the Tuanjiegou gold deposit are subordinate to the large NE-trending Wulaga Fault that hosts the gold mineralization.

The gold mineralization in the region is principally located in the NW-trending and fault-bound Early Cretaceous volcanic Sunwu–Jiayin (Armour–Jieya) Basin in the Lesser Hinggan Range. Of these, the Tuanjiegou gold deposit is hosted by the NE-trending Wulaga Fault and its NW-trending fault splay (Li et al., 2008). The orebodies are commonly located within felsic fault breccia along the contacts between felsic porphyries and the Precambrian Heilongjiang Group.

The N-treading Kuerbin Fault and its associated NS-, NE- and NNE-trending extensional faults that host the Dong'an gold deposit (Guo et al., 2004; Z.C. Zhang et al., 2010). The country rocks include the Early Cretaceous Fuminhe Formation (K_1f), consisting of rhyolitic porphyritic veins, rhyolitic tuffs, phreatic breccia, and Triassic fine- to coarse-grained K-feldspar granite. The Yanbian and Dongning Au(–Cu) mineralized belts are located to the east of Jiamusi Massif in accretionary zones along the northern margin of the NCC, and near the Dunhua and Mishan faults at the boundary of the Bulieya and Jiamusi massifs to the northeast (Fig. 1).

3. The Gaosongshan gold deposit

3.1. Geology

3.1.1. Stratigraphy of the host rocks

Volcanic units hosting the mineralization at Gaosongshan are included in the Lower Cretaceous Banzifang (K_1b) and overlying

Fig. 3. Geological map of: (a) the Lesser Xingan Range (modified from Bian et al., 2009); (b) Gaosongshan area (modified from Bian et al., 2009), and (c) simple geological profile of the Gaosongshan area.

Table 1
The features of the No. 1 Vein at the Gaosongshan gold deposit.

Vein	Orebody	Strike length (m)	Depth (m)	Dip direction (°)	Dip angle (°)	Thickness (m)			Grade (g/t)	
						Deepest	Shallowest	Mean	Highest	Mean
1	1-I	2000	440	176–205	55–72	7.9	0.49	1.41	150	5.6
	1-II	400	250	200	70	3.94	0.58	2	108.6	9.89
	1-III	400	180	95	70	1	1	1	8.42	4.97
	1-IV	1354	320	170	70–85	2.6	0.6	1.2	19.44	4.83

Ningyuancun (K_1n) formations, which have a combined thickness of ~2200 m in the Sunwu and Jiayin basins (Fig. 3). The Banzifang Formation is widespread in the mine and surrounding Sunwu and Jiayin basins covering some 1200 km^2. The formation consists of olivine basalt, basalt, basaltic andesite, andesite, trachyandesite, andesitic volcanic breccia, and pyroclastic (tuffaceous) lava (Liang et al., 2012). The Ningyuancun Formation consists of dacite, rhyolite, rhyolitic tuff and volcaniclastic rocks (Fig. 3b). The gold mineralization is closely associated with porphyritic andesite that is typically massive with a hyalopilitic matrix. The phenocrysts include 10–20 vol.% plagioclase that are up to 30 mm

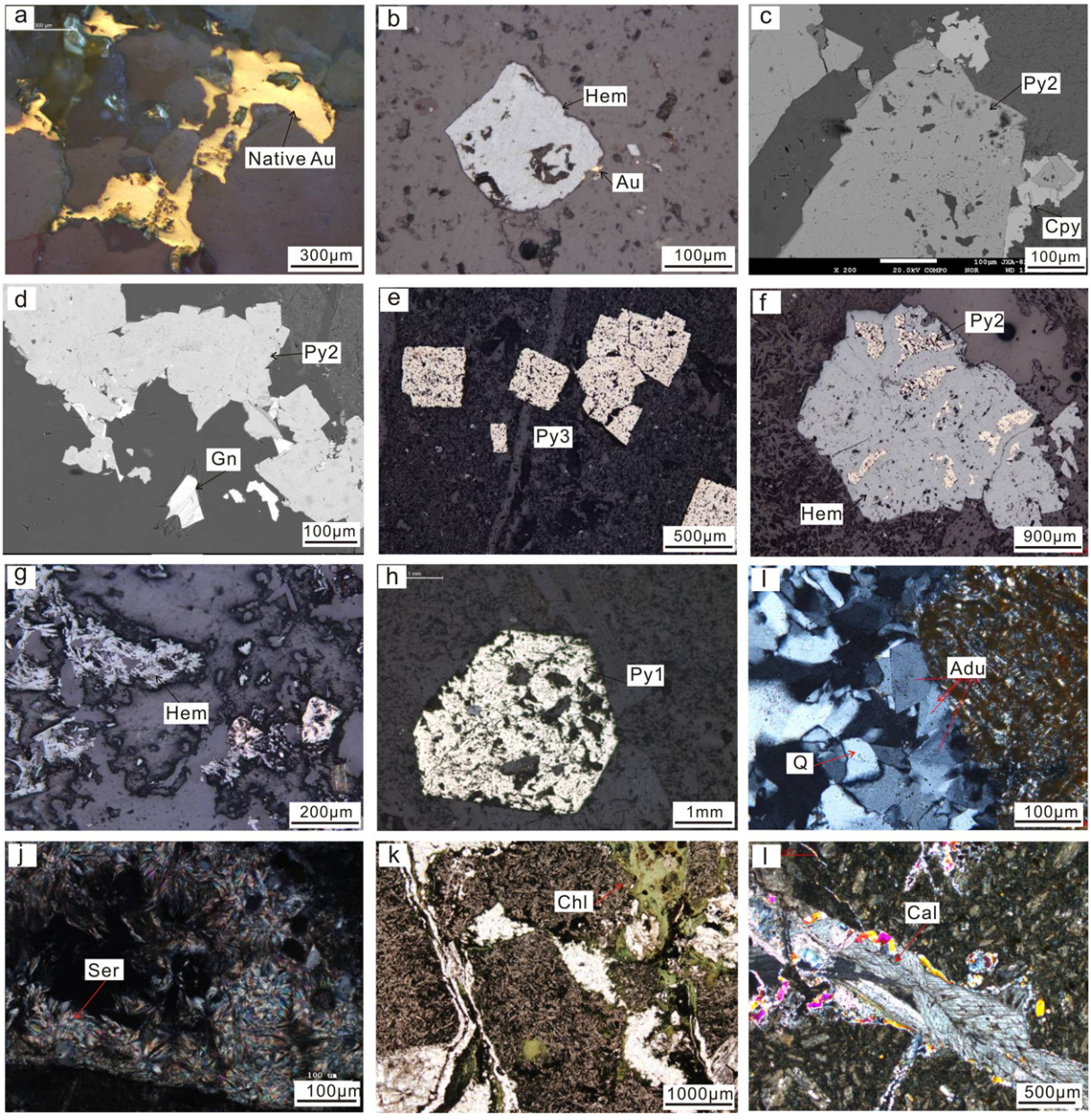

Fig. 5. Photographs of mineralization and alteration styles at the Gaosongshan gold deposit: (a) intergranular gold in andesitic breccia; (b) pyrite (Py) replaced by hematite (Hem) in quartz with visible gold; (c) Py replaced by chalcopyrite (Cpy) along the edge of pyrite in the second-stage quartz; (d) Py replaced by galena (Gn) in the second-stage quartz; (e) last stage cubic Py developed in silicified andesitic breccia; (f) second-stage Py replaced by limonite (Lim) in andesitic breccia; (g) Py replaced by Hem in andesitic breccia; (h) pentagonal dodecahedronal Py developed in andesitic breccia; (i) quartz and adularia (Adu) veins developed in andesitic breccia; (j) sericite (Ser) developed in silicified andesitic breccia; (k) chlorite (Chl) in fractures in andesitic breccia; and (l) calcite (Cal) veins in breccia.

and ~3 vol.% hornblende that are <5 mm long. The matrix is very fine-grained consisting of plagioclase, dark minerals, hyalines, and secondary epidote and zoisite (Fig. 5). Amygdales make up about 10 vol.% of the unit filled with calcite and siliceous glass with chloritized envelopes.

Structurally formed breccia is the main host for the gold mineralization at Gaosongshan and is characterized a varying grain size, which can be classified as a mortar (5–50 mm) and a finer fractured matrix. The composition of the breccia includes fragments of andesite and tuff in a siliceous, ferruginous and partially calcareous matrix. The breccia commonly contains chlorite and sericite alteration minerals and introduced pyrite.

3.1.2. Structures

The Xueshuiwen–Zhanhe, Yongqing–Gaosongshan, and Shaqihe faults control the Gaosongshan Au orebodies (Fig. 3). There are also two concealed NE-trending faults on both the southern and northern parts of the mine that have been recognized in the mine working underground and in drill holes (Lian and Wang, 2010; Zhao et al., 2011). The NE-trending Xueshuiwen–Zhanhe Fault on the northern side of the deposit is over 90 m long, and the Wuqiganxiao–Gaosongshan Fault on the southern side is 30 km long. The two faults are NE-trending extensional structures controlling the emplacement of Early Mesozoic magmatic rocks and the deposition of Mesozoic volcanic rocks in the mine area (Fig. 3a).

The NW-trending tensional Shaqihe Fault extends along the Shaqihe Valley (Fig. 3). The structure is ~7 km long and contains two tensional splays trending ENE and WNW. The ENE-trending splay is ~2 km long, up to 9 m wide, dips steeply SE, and hosts the main auriferous No. 1 quartz vein, which is locally known as the Fuqiang orebody. The WNW-trending fault is also a steep structure, and also hosts part of the No. 1 orebody, and the 2, 3 and 4 orebodies.

Volcanic structures such as concentric faults are evident on remote sensing image annular features and in diamond-drill hole core (Tang et al., 2010). Such features are present at Gaosongshan, the southern part of the Meifeng Forest, and ring structures centered on the eastward-trending faults (Fig. 3).

3.1.3. Orebodies

Detailed logging of drill holes at Gaosongshan shows that structurally prepared sites host the mineralization andesitic units (Figs. 3 and 4). Four auriferous quartz veins have been documented at Gaosongshan (Fig. 3), which are subdivided into 11 mineralized zones or orebodies (Bian et al., 2009). The orebodies are in the hanging wall of the NW-trending Shaqihe Fault at the intersections with ENE- and WSW-trending extensional shear zones forming stockworks and veins. These mineralized zones are located at shallow depth of <250 m, and the "No. 1 Vein" and "1-I" orebody being the richest with a combined metal content of 8085 kg of Au accounting for around 37% of the deposit's total resource (Table 1).

3.1.4. Mineralization and alteration

Mineralized breccia and auriferous quartz(–calcite) veins in andesite and pyroclastic host units characterize the deposit at Gaosongshan, and the sulfide content is low accounting for <1 vol.% of the ore making it a sulfide-poor type (Figs. 5 and 6). The primary metallic minerals consist of native gold, pyrite, chalcopyrite and galenite, and lesser amounts of limonite, hematite, marcasite and arsenopyrite. The primary gangue minerals are quartz, chalcedony, adularia, sericite and illite, and the non-metallic minerals include chlorite, calcite, fluorite and epidote.

Pyrite is widespread at Gaosongshan accounting for up to 2 vol.% of the ore. The pyrite typically has a diameter of 0.1–0.8 mm, and

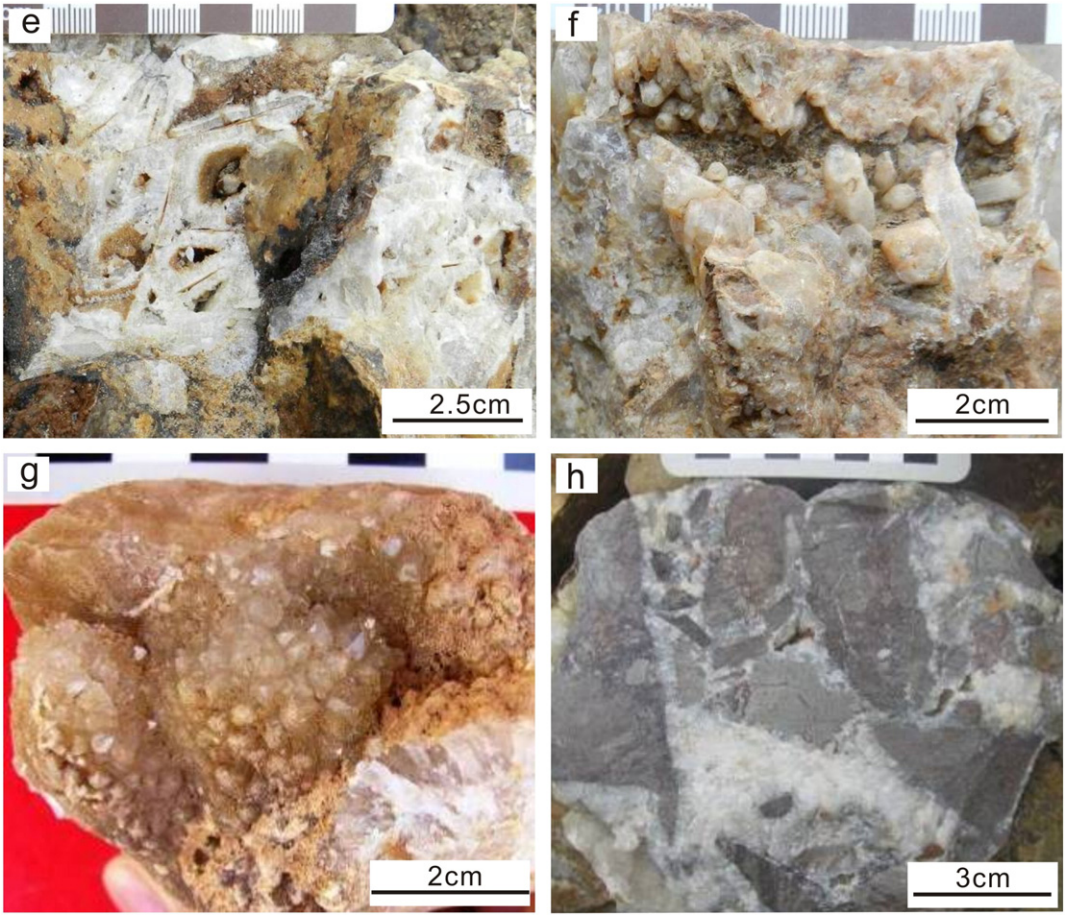

Fig. 6. Ore structural textures at the Gaosongshan gold deposit: (a) bladed quartz structure; (b) comb structure; (c) drusy structure; and (d) breccia.

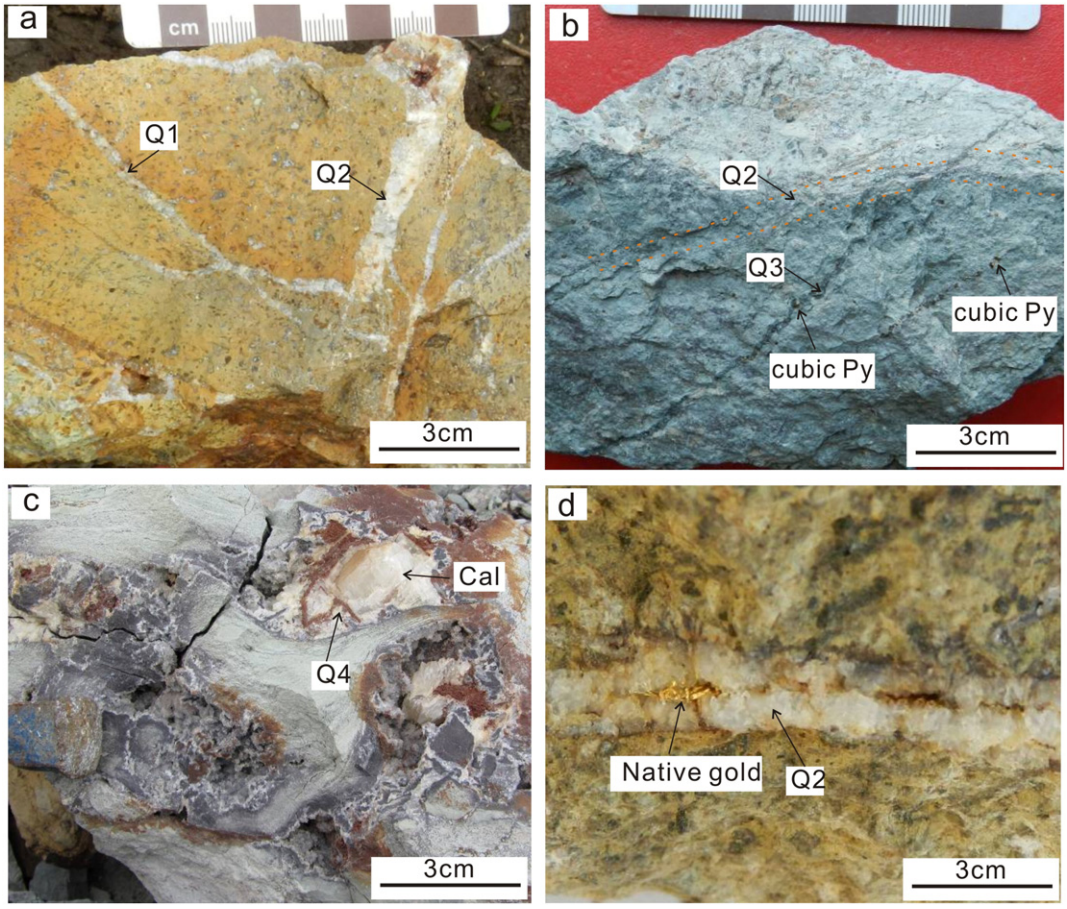

Fig. 7. Mineralization stages in the Gaosongshan gold deposit: (a) First-stage quartz; (Q) vein cut by a second-stage quartz vein developed in silicified andesite; (b) second-stage quartz vein cut by a third-stage quartz vein containing cubic pyrite (Py) in chloritized andesitic units; (c) late-stage quartz (Q4) and calcite (Cal) vein; (d) second-stage quartz veins with native gold in andesite containing phenocryst, vesicular and amygdaloidal structures.

two generations have been identified. The early pyrite is euhedral to subhedral and few of the grains are star-shaped. These grains are commonly present as disseminated crystals with magnetite and ilmenite in the andesitic rocks (Fig. 5h), and are variably pseudomorphed by hematite and limonite or overgrown by galena, chalcopyrite, marcasite and arsenopyrite. The second generation of pyrite is subhedral-granular and anhedral in shape, and is present in quartz veins where it is closely associated with native gold (Fig. 5c–f). Chlorite and sericite commonly overgrows the pyrite (Fig. 5c). The gold is hosted by drusy quartz in the breccia, and rare galena, marcasite and adularia are also present in the breccia overgrowing pyrite.

Wall rock alteration is zoned outward from mineralized zones at Gaosongshan (Figs. 4 and 5). The central part of the alteration is characterized by the assemblage silica–adularia–pyrite, which is succeeded by sericite–illite–chlorite–pyrite and then chlorite–epidote–carbonate–fluorite along the outer edges.

The silica alteration forms cement in the mineralized breccia or as stockwork and individual veins, which are crosscut by auriferous quartz(–adularia) veins. It is here suggested that the quartz paragenesis represents a progress single event associated with the gold deposition. The later stage is also associated with chlorite, illite, sericite, epidote and carbonate.

Adularia forms euhedral–subhedral platy and rhombic crystals with a diameter of <0.1 mm, mainly distributed at the contact between the late-stage quartz with the mineralized breccia. In addition, sericite alteration is intense and associated with the late stage quartz representing phyllic alteration accompanied by pyrite. Chlorite commonly forms veins infilling fractures in the wall rocks or replacing augite and olivine in the volcanic. Illite is well developed near the silica–adularia alteration zones and is accompanied by pyrite and sericite.

Finally, from the cross-cutting relationship of the mineralized veins (Fig. 7), in combination with ore fabrics, mineral paragenesis and the relationships of various minerals with gold mineralization discussed above, Gaosongshan can be classified as hydrothermal deposit that has been supergene enriched at shallow depths (Fig. 8).

3.2. Mineral assemblages

The mineral assemblages in the alteration zones have been determined based on petrology, paragenetic studies, and detailed geochemical

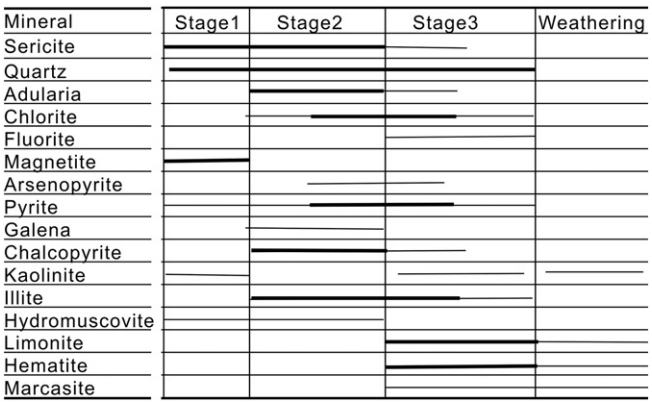

Fig. 8. Mineral paragenetic scheme for the Gaosongshan gold deposit.

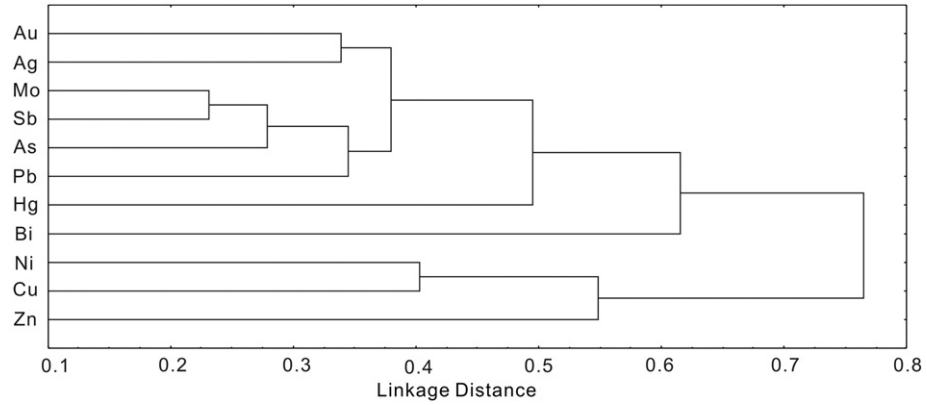

Fig. 9. Diagram of element cluster analysis.
From Hao (2013).

analyses using the R-type cluster analysis of 278 samples at Gaosongshan (Hao, 2013).

When the distance coefficient is <0.5, the elements can be grouped into four groups: (1) Au–Ag–Mo–Sb–As–Pb–Hg; (2) Bi; (3) Cu–Ni; and (4) Zn (Fig. 9). The Au–Ag–Mo–Sb–As–Pb–Hg group is a low-temperature association typical of epithermal mineralization and probably related to magma, given the presence of volcanic host rocks. The second group (Bi) commonly has a magmatic orogen indicative of medium- to high-temperature conditions and is commonly associated with gold (Ciobanu et al., 2009). The third and fourth groups are dominated by the high-temperature elements Cu, Ni and Zn, which are commonly associated with intermediate and mafic rocks.

3.3. Fluid inclusion study

The quartz hosted by andesite and breccia contains abundant fluid inclusions. The quartz forms well-developed crystals containing isolated groups of inclusions. Fluid inclusions in quartz in the mineralized breccia hosted by pyroclastic units are very small and commonly isolated. Auriferous quartz contains 4–25 μm wide primary gas–liquid inclusions with gas bubbles occupying 5–25% in the early fluid-rich inclusions 50–80% in the relatively later vapor-rich inclusions.

Primitive inclusions are best developed in the early mineralization quartz, and are often water-rich inclusions. In the late-stage mineralization quartz, the primitive inclusions, often as the vapor-rich ones, are a little smaller, but the homogeneous temperature is mostly higher. The general homogenization temperature for both types of inclusions is ≤320 °C, with a salinity of <7 wt.% NaCl and a density of <1 g/cm^3. These characteristics suggest that the mineralization took place at depths of between 430 and <1000 m (Fig. 10). On passing, the two types of inclusion studied at Gaosongshan (i.e. liquid dominant and gas dominant) could be due to fluid boiling (suggesting that the mineralizing event was at least partly driven by changes in fluid pressure).

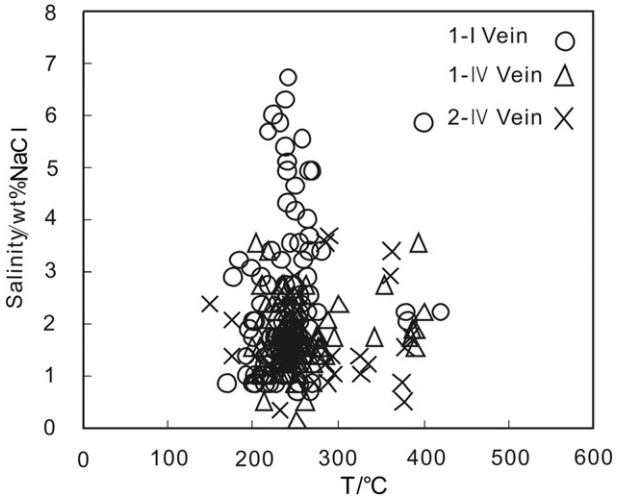

Fig. 10. Homogenous temperature versus salinity plots for liquid inclusions in auriferous quartz.
Data after Hao (2013).

4. Analytic methods

Samples were collected for H–O–S–Pb isotope analysis principally from the No. 1 and No. 2 veins at Gaosongshan (Fig. 3; Tables 2–4), samples of quartz were collected for H–O isotope analysis from various auriferous quartz veins at the deposit, and samples of pyrite were collected and sieved through a 200 mesh for S and Pb analyses. Five samples of pyrite were collected from ore and mineralized wall rocks for sulfur isotope.

Analyses were done using a MAT253-type mass spectrometer at the Isotopic Laboratory at the China Nuclear Industry Geological Research Institute using the Standard Mean Ocean Water (VSMOW) as a water standard. The analytic precision (2σ) of H_2 is ±1‰, and the O_2 (2σ) exceeds ±0.2‰.

Lead isotopic ratios were measured with the British-made Nu Plasma HR multi-receiver MC-ICPMS. The mass fractional distillation was corrected by the external standard of T1 isotope (He et al., 2005). The statistical result of long-term measurement of Pb standard sample NBS981 is $^{207}Pb/^{206}Pb = 0.91488 \pm 0.00028$.

Table 2
Hydrogen and oxygen isotope composition of ore from the Gaosongshan gold deposit.

Samples	Mineral	$\delta^{18}O_{quartz}$ (‰)	Temperature (°C)[a]	$\delta^{18}O_{H_2O}$ (‰)[b]	δD_{H_2O} (‰)
GB-I-4	Quartz	3.4	250	−5.5	−111.3
GB-I-49	Quartz	6.1	250	−2.8	−111.6
GB-I-68	Quartz	4.4	250	−4.5	−111
GB-2IV-63	Quartz	5.9	260	−2.55	−125.3
GB-2IV-65	Quartz	3.8	260	−4.65	−118.4
GB-IV-48	Quartz	5.1	245	−4.04	−119.2
GB-IV-55	Quartz	4.6	245	−4.54	−123.8
B-31*	Quartz	3.3	260	−5.60	−124
B-34*	Quartz	4.1	248	−4.71	−120
B-35*	Quartz	3.4	252	−5.41	−129
B-37*	Quartz	3.2	249	−5.61	−117
B-38*	Quartz	2.7	252	−6.11	−118

Note: Sample B* is from Bian et al. (2009).
[a] Model temperature as determined from the fluid inclusion homogenization temperatures.
[b] Calculated $\delta^{18}O$ fluid composition determined using the isotope fractionation equation $10^3 \ln\alpha_{quartz-water} = 3.34 \times 10^6/T^2 - 3.31$ (Matsuhisa et al., 1979).

Table 3
Sulfur isotope composition of the Gaosongshan gold deposit.

Pyrite sample	From	$\delta^{34}S_{CDT}$ (‰)
GT11-I-1	Brecciated tuff; ore	0.3
GT11-2IV-6	Brecciated tuff; ore	−2.4
GT11-III-7	Brecciated andesite; ore	0.3
GF11-I-49	Brecciated andesite; ore	0.4
GB11-2IV-65	Brecciated andesite; ore	−0.3
Y-4*	Ore and mineralization wall rock	1.6
Y-8*	Ore and mineralization wall rock	1.9
Y-11*	Ore and mineralization wall rock	1.7
B-2*	Ore and mineralization wall rock	2.9
B-3*	Ore and mineralization wall rock	1.8
B-4*	Ore and mineralization wall rock	1.2
B-14*	Ore and mineralization wall rock	2
B-15*	Ore and mineralization wall rock	2.8
B-21*	Ore and mineralization wall rock	1.5
B-23*	Ore and mineralization wall rock	1.2
B-25*	Ore and mineralization wall rock	2.3

Note: Sample* is from Bian et al. (2009).

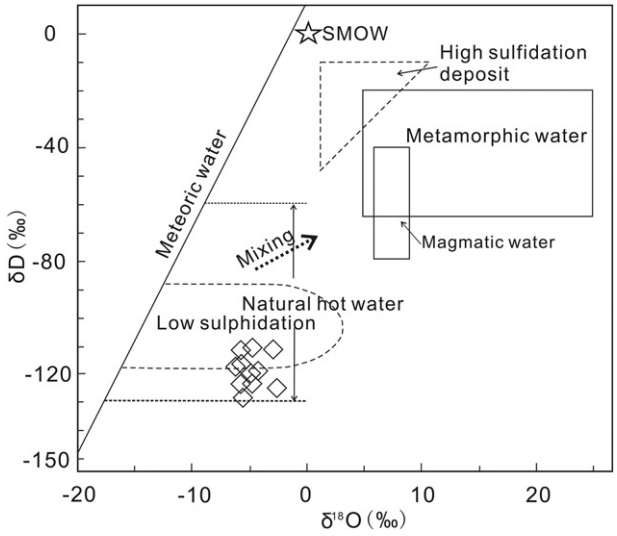

Fig. 11. Diagram showing $\delta^{18}O$‰ vs δD‰ for mineralizing fluid at the Gaosongshan gold deposit.
After Hedenquist and Lowenstern (1994).

The analytical preparations included: (1) hydrogen and oxygen isotope analysis using fluid inclusions from seven samples; (2) quartz samples were sieved using 40–60 meshes and degassed in a vacuum at a temperature of 150 °C for over 4 h in order to thoroughly remove surface and interstitial water; (3) the samples were then crusted and heated to 400 °C to extract fluid from inclusions, which caused it to react with zinc to produce H_2; (4) O_2 was produced by the reaction of quartz with BrF_5, and the SiF_4 and BrF3 impurities were separated using the refrigerant method; (5) CO_2 was generated using a platinum activator at 700 °C after the reaction between O_2 and graphite, and then collected using the refrigerant method; and (6) sulfur analyses were completed on pyrite samples sieved using a 200-mesh with pure $BaSO_4$ being extracted using the Eschkas reagent, and SO_2 was generated using V_2O_5 or Cu_2O; the analytical accuracy is ±0.2‰ (2σ) using the V-CDT standard.

Laser ablation inductively coupled mass spectrometry (LA-ICP-MS) zircon U–Pb dating was completed on samples from the auriferous No. 1 quartz vein (Figs. 3 and 15a). The samples were crushed using a 60 mesh and concentrated after gravity and magnetic sorting. Over 100 zircons were mounted for each sample and imaged under transmitted light and cathodoluminescence (CL) for microscopic analysis of the internal texture of the zircon grains. The dating was completed at the Key Laboratory of Metallogeny and Mineral Assessment of the Institute of Mineral Resources Chinese Academy of Geological Sciences. A Finnigan Neptune and New wave UP 213 denudation system were applied using a laser frequency of 10 Hz, a laser diameter of 25 μm and a denudation depth of 20–40 μm. The GJ-1 zircon was analyzed as an external standard, and the M127 zircon was used as a standard for U and Th concentrations (U: 923 ppm; Th: 439 ppm; Th/U: 0.475; Nasdala et al., 2008). The ICPMSDataCal software of Liu et al. (2010) was run for data processing. Normal Pb correction was not conducted in most analytical points with $^{206}Pb/^{204}Pb > 1000$. Concordia diagrams and weighted mean calculations were made using Isoplot/Ex_ver3 (Ludwig, 2003). The detailed experiment and test methodology follow those of Hou et al. (2009).

5. Analytical results

5.1. Hydrogen and oxygen isotopes

The $D_{V\text{-}SMOW}$ value for ore at Gaosongshan ranges from −129 to −111‰ (Table 2), and the $^{18}O_{fluid}$ value varies between ~7.9 and 13.8‰. These variations for the mineralizing fluid are limited and plot in the meteoric water field on Fig. 11, which are typical of fluids associated with low-sulfidation type epithermal deposit (Hedenquist and Lowenstern, 1994). Furthermore, the relative-low δD value might be related to degassing of boiling fluid (Giggenbach, 2003).

5.2. Sulfur isotope

The sulfur isotope data are listed in Table 3. The $\delta^{34}S$ values of the pyrite samples from ore at Gaosongshan have a narrow range between −2.4 and 2.9‰ (Fig. 12). This narrow range suggests that the sulfide in the ore crystallized during stable physical and chemical conditions, in addition to a relatively uniform sulfur source (Zhang et al., 1981).

5.3. Lead isotopes

The lead isotope compositions of the pyrite samples from ore at Gaosongshan are listed in Table 4. These values are higher than those from mantle values (i.e. $^{206}Pb/^{204}Pb = 18.01$, $^{207}Pb/^{204}Pb = 15.42$, and $^{208}Pb/^{204}Pb = 37.70$; Doe and Zartman, 1979). The $^{207}Pb/^{204}Pb$ value for feldspar from a mantle source is generally lower than 15.60, whereas the values for crustal and mixed mantle-crustal sources are generally >15.60 (Shen, 1997). The $^{207}Pb/^{204}Pb$ value for lead from the ore is between 15.14 and 15.69, which is close to the upper limit for a mantle source.

Table 4
Lead isotope compositions and characteristic values in the Gaosongshan gold deposit.

Sample	$^{206}Pb/^{204}Pb$	2σ	$^{207}Pb/^{204}Pb$	2σ	$^{208}Pb/^{204}Pb$	2σ	t (Ma)	μ	ω	Th/U
GT-I-1	18.137	0.001	15.514	0.001	38.005	0.003	259.80	9.32	35.42	3.68
GT-2IV-6	18.394	0.002	15.569	0.002	38.227	0.004	139.80	9.4	35.46	3.65
GT-III-7	18.382	0.002	15.563	0.002	38.201	0.004	141.10	9.39	35.37	3.65
GF-I-49	18.147	0.002	15.515	0.002	38.395	0.005	253.70	9.32	37	3.84
GB-2IV-65	18.459	0.002	15.568	0.002	38.28	0.004	90.60	9.4	35.33	3.64

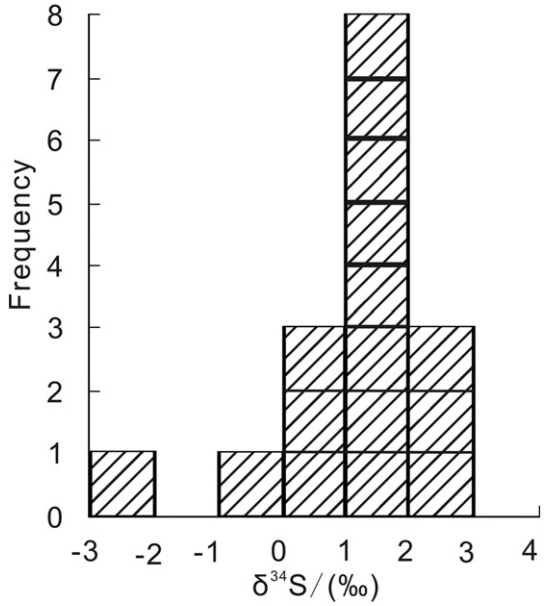

Fig. 12. Sulfur isotope composition for the Gaosongshan gold deposit.

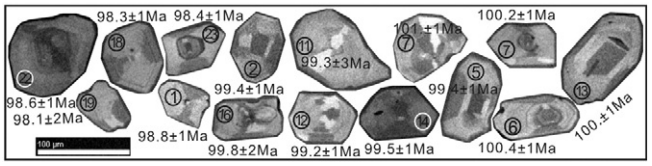

Fig. 14. Cathodoluminescence (CL) images for zircons from auriferous quartz veins at the Gaosongshan gold deposit.

The various plots for the lead isotopes in Fig. 13 indicate that the lead associated with the mineralization indicates that the lead is derived from the mantle or is associated with an orogenic tectonic setting, and the lead with the mantle source has an evolved growth curve (Fig. 13c, d).

In general, lead derived from the upper mantle or lower crust has μ values of 8.92–9.06, W values of 35–41, and Th/U ratios of 3.83–4.01. In contrast, the continental crust has average μ values of 9.0 and Th/U ratios of 4.1, whereas ore from Gaosongshan has higher μ values of 9.3–9.46 and lower Th/U ratios of 3.67–3.86 (Table 4). In addition, the lead model ages for the ore form two distinct groups with dates of ca. 260–253 and 141–91 Ma.

5.4. Metallogenetic chronology

Samples of auriferous quartz were collected from the No. I vein at Gaosongshan for geochronological studies (Fig. 3). Judging from the CL images, the zircons extracted from the quartz have clouded edges, are 40–100 μm in diameter, have long platy structures, and are well-rounded or are irregular in shape (Figs. 14 and 15a). The zircons typically have cores that are discordant from their rims, which are interpreted as secondary hydrothermal growths on inherited cores (e.g. grains 6, 16, 17, 22 and 23 in Fig. 14). The rims are also interpreted as being synchronous with the gold mineralization, which have relatively high Th/U values ranging from 0.59 to 1.54 and dates between ca. 101 and 98 Ma

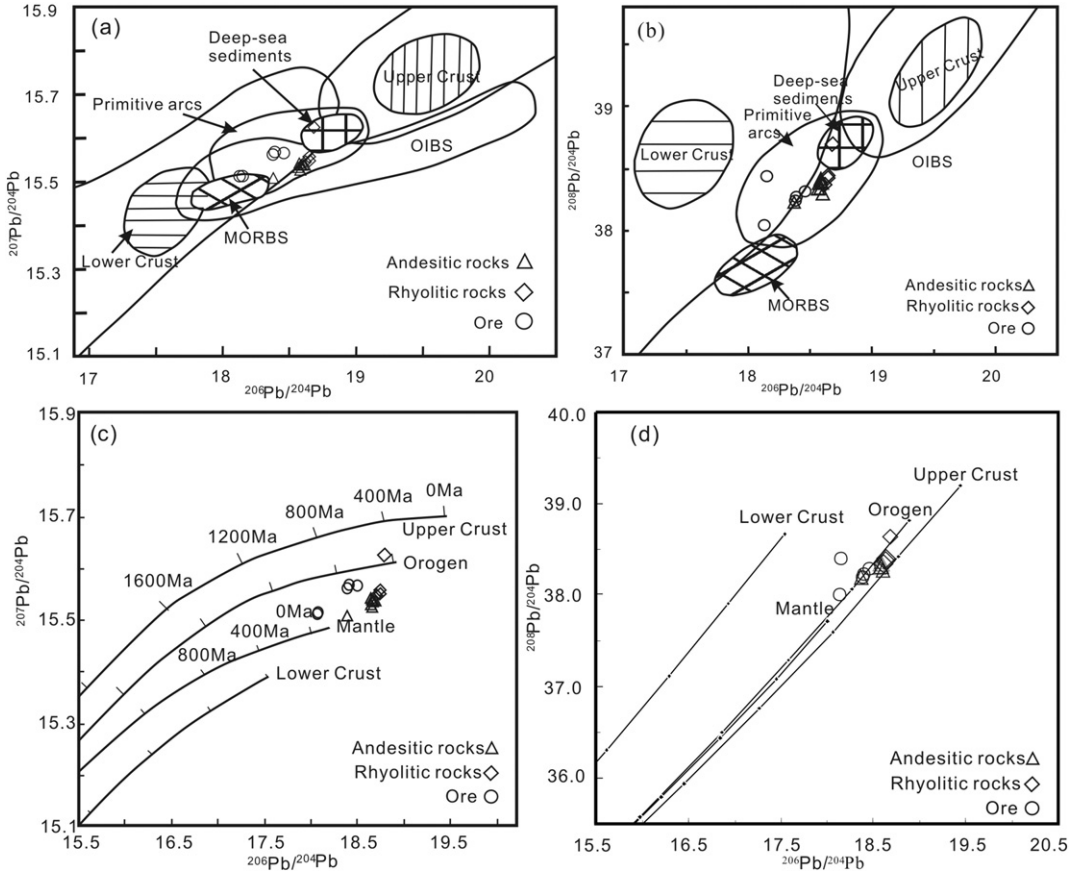

Fig. 13. Sulfide lead isotope mode diagram for the Gaosongshan gold deposit (after Zartman and Doe, 1981). Data for the andesitic and rhyolitic rocks are from Hao (2013). (a, b) Samples of ore and wall rock all fall into the range of primitive arcs, and the ore is closer to andesitic rock, the MORB fields and lower crust; (c, d) samples of ore and wall rock all fall into the range of orogene and mantle, and the ore is closer to andesitic rock, the mantle and the lower crust, and with older model age.

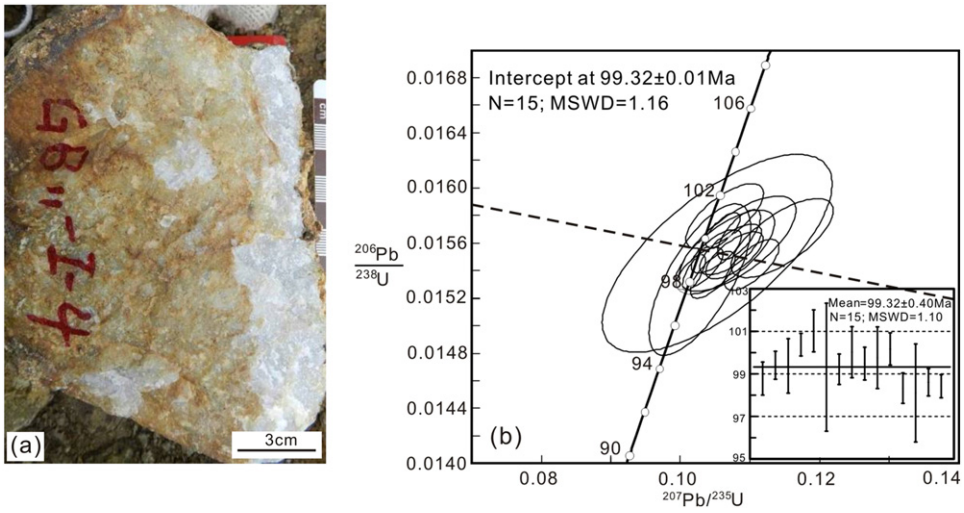

Fig. 15. Samples from the Gaosongshan gold deposit of: (a) auriferous quartz veins; and (b) zircon LA-ICP-MS U–Pb concordia plots.

(Table 5). The weighted average age for the rims is 99 ± 1 Ma (n = 15, MSWD = 1.1), which is the same as the concordant age of 99 ± 1 Ma (n = 15, MSWD = 1.16). Given that this date is slightly younger than the ca. 102 Ma date for the host andesite and andesitic tuff that is capped by the non-mineralized ca. 97 Ma rhyolite (Hao, 2013), the ca. 99 Ma date is interpreted as an accurate age for the gold mineralization.

6. Discussion

6.1. Deposit type

Through systematic comparative study (Table 6), Gaosongshan can be classified as a typical low-sulfidation type epithermal deposit.

6.2. Source of metals

Near-surface volcanism associated with the epithermal gold is related to calc-alkaline units such as basaltic andesite, andesite, dacite and rhyolite, and calc-alkaline magmatism is commonly associated with subduction and gold mineralization (e.g. Sillitoe, 1993). The $\delta^{34}S$ value for the pyrite from the mineralization at Gaosongshan has a narrow range between −2.4 and 2.9‰, which is similar to that of mid-ocean ridge basalt (MORB) deep magmatic sulfur, and consistent with many magma-related deposits with values between −3 and 1‰ (Hoefs, 2009).

Lead isotope studies suggest that gold is associated in the Lesser Hinggan Range with the continental-margin arc-magmatism west of the Paleo-Pacific plate (Zhou et al., 2009b; Zhang et al., 2012; Xu et al., 2013). Relics of the magmatic-arc associated with back-arc subduction act as the source for strong sulfurphile elements such as Au, which are accompanied by Cu mineralization (Richards, 2011).

The host-wall rocks at the Gaosongshan, Dong'an and Tuanjiegou gold deposits have a source from newly generated lower crust with the andesitic units having εNd(t) values of 0.3–2.4 and the younger rhyolitic units having εNd(t) values of −0.2 to −3.05 (Z.C. Zhang et al., 2010; Hao, 2013). In addition, the felsic rocks in the region contain more crust-derived material.

The Pb-isotope values ($^{207}Pb/^{204}Pb$ = 15.14–15.69; μ = 9.3–9.46 and Th/U = 3.67–3.86) for ore in the Lesser Hinggan Range that are consistent with those of andesitic and rhyolitic rocks that have mantle sources (Fig. 12). However, the Pb in the ore also has a lower crustal source and its Pb model age is older (i.e. 260–253 Ma). Generally, sulfides in the ore have higher Pb-isotope ratios than the andesitic and rhyolitic rocks implying that the lead in the ore has a source other than the andesitic and rhyolitic rocks, and that source might be an enriched lithospheric mantle and lower crust (Fig. 12).

Lead, ore sulfide and wall rocks plot in the orogenic tectonic field in Fig. 13, but the sulfide samples also plot near those of the andesitic rocks and partly in the MORB field. In addition, the Th/U ratio is lower than that of normal Pb from the lithospheric mantle and lower crust, which suggests that it has an abnormally higher radioactive Pb and U content, and is deficit in Th. These characteristics are similar to those of Paleozoic rocks in the Central Asia Orogen, which are characterized abnormally high μ values (Shao et al., 2010). The higher μ values might be related to the lithospheric mantle being replaced by, or mixed with, the middle to upper crust with higher U and Th values (Taylor and McLennan, 1985).

The older Pb model age of ca. 260–253 Ma for pyrite from the ore at Gaosongshan is broadly concordant with the Late Permian age of the Central Asian Orogen forming the basement in the Zhangguangcai and Lesser Hinggan ranges (Wu et al., 2011). The younger Pb model age of ca. 141–90 Ma for pyrite from the ore is broadly synchronous with the ca. 102–97 Ma age of the wall rocks and the Early Cretaceous mineralization age of 99 Ma. This indicates that the pyrite has a mixed source including the crust and the lithospheric mantle.

6.3. Metallogenetic fluid migration and mineral enrichment

Low-sulfidation epithermal gold deposits are usually further from intrusions than high-sulfidation deposits (Hedenquist and Lowenstern, 1994). If low-sulfidation deposits are distally related with intrusion, their ore-forming gaseous-fluid must have been moved over relatively long distances, which would require fluid migration through large-scale faults, such as the Shaqihe Fault (Hao, 2013).

Fresh samples were collected at Gaosongshan for an R-type cluster analyses of their Au, Ag, As, Sb, Hg, Cu, Mo and Pb content, and to compile equal-value element maps along longitudinal sections (Figs. 8 and 16). By doing this, it is evident that Sb–Hg is significantly elevated at depth to the east of the deposit near the Shaqihe Fault and gradually decreases to shallow depth to the west (Fig. 16). The higher temperature assemblage of Cu–Pb–Ag is elevated in the central and shallow parts of the longitudinal sections. The high-temperature elements (Au–As, Mo) are situated in the shallow western part of the study area (Fig. 16). These observations suggest that the mineralization proceeded from deeper depths in the east to a shallow depth in the west. These observations also suggest that the Shaqihe Fault was the main conduit for the mineralizing fluid, and that the ore developed in the SW hanging wall of the fault.

Table 5
Zircon LA-ICP-MS U–Pb analytical results for auriferous quartz vein GB-I-4 from the Gaosongshan gold deposit.

Samples	^{232}Th (10^{-6})	^{238}U (10^{-6})	Th/U	$^{207}Pb/^{206}Pb$	±1σ	$^{207}Pb/^{235}U$	±1σ	$^{206}Pb/^{238}U$	±1σ	$^{208}Pb/^{232}Th$	±1σ	$^{207}Pb/^{206}Pb$	±1σ	$^{207}Pb/^{235}U$	±σ	$^{206}Pb/^{238}U$	±σ	$^{208}Pb/^{232}Th$	±σ
GB-I-4-1	80.731	85.829	0.941	0.052	0.0012	0.110	0.0026	0.015	0.0001	0.0027	0.0004	279.69	49.07	106.2	2	98.8	1	53.6	8
GB-I-4-2	51.194	62.569	0.818	0.049	0.0011	0.105	0.0024	0.016	0.0001	0.0038	0.0005	150.09	56.47	101.5	2	99.4	1	77.6	9
GB-I-4-5	39.239	56.210	0.698	0.050	0.0022	0.106	0.0047	0.016	0.0002	0.0061	0.0008	183.42	101.84	102.7	4	99.4	1	122.3	15
GB-I-4-6	50.574	80.002	0.632	0.049	0.0007	0.106	0.0016	0.016	0.0001	0.0038	0.0005	150.09	32.41	102.4	2	100.4	1	76.2	9
GB-I-4-7	49.175	81.033	0.607	0.050	0.0018	0.106	0.0037	0.016	0.0002	0.0039	0.0009	146.38	85.17	102.6	3	101.0	1	78.5	19
GB-I-4-11	39.197	57.569	0.681	0.049	0.0048	0.105	0.0109	0.016	0.0005	0.0004	0.0000	166.75	205.53	101.6	10	99.3	3	7.8	1
GB-I-4-12	40.811	57.772	0.706	0.050	0.0012	0.108	0.0027	0.016	0.0001	0.0062	0.0008	209.33	53.69	103.9	2	99.2	1	125.1	16
GB-I-4-13	42.231	62.727	0.673	0.053	0.0023	0.115	0.0048	0.016	0.0002	0.0050	0.0011	338.95	98.14	110.2	4	100.1	1	100.5	22
GB-I-4-14	60.074	74.026	0.812	0.050	0.0014	0.102	0.0029	0.016	0.0001	0.0039	0.0005	198.23	30.55	103.4	3	99.5	1	78.8	10
GB-I-4-16	30.350	51.694	0.587	0.051	0.0028	0.108	0.0055	0.016	0.0002	0.0072	0.0018	220.44	127.76	104.3	5	99.8	2	144.5	35
GB-I-4-17	48.790	71.702	0.681	0.050	0.0010	0.108	0.0020	0.016	0.0001	0.0055	0.0008	209.33	44.44	104.5	2	100.2	1	109.9	15
GB-I-4-18	43.428	65.722	0.661	0.049	0.0010	0.105	0.0021	0.015	0.0001	0.0058	0.0008	168.60	46.29	101.1	2	98.3	1	116.8	16
GB-I-4-19	52.749	75.999	0.694	0.050	0.0027	0.138	0.0048	0.015	0.0004	0.0049	0.0016	200.08	69.44	99.3	4	98.1	2	99.7	32
GB-I-4-22	42.662	62.117	0.687	0.048	0.0010	0.103	0.0022	0.015	0.0001	0.0069	0.0007	120.46	45.37	99.3	2	98.6	1	139.4	14
GB-I-4-23	383.30	248.214	1.5442	0.048	0.0005	0.102	0.0011	0.015	0.0001	0.0011	0.0001	101.94	24.07	98.6	1	98.4	1	22.5	2

Mineralizing fluids associated with low-sulfidation type epithermal gold deposits are usually characterized by temperatures of <300°, low salinities of <3.5 wt.% NaCl, and meteoric water fluids with reducing, near neutral pH values (Hedenquist et al., 2000; Corbett, 2002). In these fluids, the sulfides are predominantly in the form of $H_2S_{(aq)}$ and Au is transported as an $Au(HS)_2^-$ complex. Gold is commonly deposited during pressure drops associated with boiling, and during fluid mixing with groundwater containing low-valence reducing sulfur and sulfate leading to the instability of reduced sulfur (Cooke and Simmons, 2000; Simmons and Browne, 2000).

In most low-sulfidation epithermal deposits, mineral assemblages and textures such as bladed calcite, quartz with a lattice shape, adularia, and the relatively narrow vertical distribution and spatial fluctuation in ore hosted by quartz veins are characteristic of boiling and release of H_2S gas (Brown, 1986).

Fluid inclusion studies indicate that the mineralizing fluid at Gaosongshan is characterized by low temperatures between 150° and 310 °C, low salinities of 0.7–3.71 wt.% NaCl, and lower densities of 0.48–0.94 g/cm^3. The gaseous components include CO_2, CO, N_2CO, and minor amounts of CH_4, C_2H_2, C_2H_4 and C_2H_6, and a significant proportion of these gases (CH_4, C_2H_6, CO_2, CO and N_2) are reducing (Hao, 2013). Furthermore, the composition of the fluid in the fluid inclusions associated with the mineralization includes the ions Ca^{2+}, Mg^{2+}, K^+, Na^+, SO_4^{2-}, Cl^- and NO_3^-, which are common in meteoric solutions (Hao, 2013; Robb, 2005).

Mineralizing fluid and wall rocks should reach a chemical balance for low-sulfidation epithermal deposits formed at depths of <2 km (Rowland and Simmons, 2012). The pH of the fluid is buffered and neutralized by alkaline minerals such as albite–K-feldspar–muscovite from the country rocks if the S content is greater than the Fe content. Fluid inclusions interpreted to represent the mineralizing fluid at Gaosongshan are characterized by their sulfide content of <0.5 vol.%, and gold is dominantly hosted by quartz and adularia veins. The gold commonly fills intergranular spaces in the second-stage of quartz forming granular gold and electrum (62.8–71.8 wt.% Au, and 26.5%–34.7 wt.% Ag) and in pyrite that is commonly altered to hematite and limonite (Fig. 17). In addition, disseminated pyrite is common in altered rocks in deeper sections at the No. 1-IV and 2-IV veins near the Shaqihe Fault. Therefore, gold was transported in low-salinity brines in the area as a $Au(HS)_2^-$ complex at low temperatures of 150°–310 °C, and neutral pH. This is represented by the equations:

$$2Au + 4H_2S = 2Au(HS)_2{}^- + 2H^+ + H_2; \text{ and} \quad (1)$$

$$2Au + 2H^+ + 4HS^- = 2Au(HS)_2{}^- + H_2. \quad (2)$$

In general, gaseous components in mineralizing fluids are commonly derived from magmatic fluids originating from deep intrusions (Henley, 1990; Pudack et al., 2009). Generally, K, Na, Fe, Pb and Zn have similar fractionation behaviors and are preferably present in brines (Seo et al., 2009). Sulfur is in a relatively more volatile gas compared with Fe and Cu, and in the gaseous phase it carries Au, Mo, As and Cu in reducing conditions (Heinrich et al., 1992; Seo et al., 2009). These elements can be separated from Fe-rich brines at depth (Heinrich et al., 2004), and gold is liberated from such fluids following the equation:

$$Au^+ + Fe^{2-} + 2HS^- = Au + FeS_2 + 2H^-. \quad (3)$$

However, this reaction cannot be the main way for gold to be precipitated at Gaosongshan due to its low-sulfide content, although gold is locally present in pyrite in breccia and altered wall rocks. This seems to result in the instability of reducing sulfur with low-valence reducing sulfur and ground water according to the reaction:

$$H_2S + 3H_2SO_4 = 4SO_2 + 4H_2O. \quad (4)$$

Table 6
Comparison between the Gaosongshan gold deposit and a typical low-sulfidation epithermal deposit.

Items	Low-sulfidation epithermal deposit	Gaosongshan gold deposit
Tectonic setting	Arc and back-arc settings with the subduction of the plate	Arc-back stretching and rift zones in the continental side of the active continental margin
Magmatism	Calc-alkaline igneous rock, continental facies	Calc-alkaline continental (arc)
Host rock	Andesite (basalt)–dacite–rhyolite	Andesite, basaltic andesite and andesitic tuff
Ore-controlling structure	Steep dilation structure related to volcanism	NE-striking tensional and shearing Shaqihe Fault and eastward trending tensional splay structures
Mineralized ages	Predominant Cretaceous and Cenozoic	Cretaceous (99 Ma)
Ore body occurrence	Steep vein	Steep vein
Ore mineral compositions	Generally, metal mineral including pyrite, pyrrhotite, arsenopyrite, sphalerite and galena; gangue mineral: quartz, chalcedony, calcite, adularia, sericite and illite	Dominant metal mineral: native gold, pyrite, hematite, limonite, with less galena, chalcopyrite and arsenopyrite; non-metal mineral; quartz, chalcedony, calcite, adularia, sericite, illite, epidote and chlorite
Ore fabric	Banded, drusy, vuggy, nodular and crustal, lattic and brecciated structure	Brecciated, drusy, vuggy, blade, coliform, nodular and crustal structure; and anhedral granular, flake, replacement remnant texture
Wall-rock alteration	chalcedony, adularia, illite, montmorillonite, sericite	Silica, chalcedony, adularia, illite, sericite, montmorillonite, chlorite, epidote, carbonate
Element assemblages	Au, Ag, As, Sb, Zn, Pb, Hg	Au, Ag, As, Sb, Pb, and minor Cu, Hg, Mo
Metallogenic temperature	Minor 100°–320°	Dominant 150°–310°
Liquid salinity	0–10 wt.% NaCl	0.7–3.71 wt.% NaCl
Mineralization depth	Less than 1.5 km	Mainly concentrated in 430–830 m
H–O isotope	Meteoric water	Meteoric water
S isotope	Magmatic sulfur	Magmatic sulfur

Epithermal deposit after Cooke and Simmons (2000), Jiang et al. (2004) Simmons and Browne (2000), Simmons et al. (2005).

This would result in gold deposited and the production of acidic fluids. Consequently, quantities of argillite and the special alteration mineral assemblages of kaolinite–alunite–pyrophyllite would be produced in the corresponding acidic and oxidized environments. However, these reactions do not account for the neutral pH and low-temperature alteration minerals of bladed quartz, sericite, adularia, calcite, and chlorite present at Gaosongshan, which are crystallized under the following reactions:

$$3NaAlSi_3O_{8(albite)} + K^+ + 2H_2O = KAl_2[AlSi_3O_{10}](OH)_{2(sericite)} + 6SiO_{2(quartz)} + 3Na^+ + 2H^+ + O_2; \quad (5)$$

$$3CaAlSi_3O_{8(plagioclase)} + K^+ + 4H_2O = 2KAl_2[AlSi_3O_{10}](OH)_{2(sericite)} + 6H_2O + 3Ca^+ + 4H^+ + 2O_2; \quad (6)$$

$$Ca^{+2} + 2HCO_3{}^- = CaCO_{3(calcite)} + CO_2 + H_2O; \quad (7)$$

$$KAl_3Si_3O_{10}(OH)_{2(sericite)} + 6SiO_2 + 2HCO_3{}^- + 2K^+ = 3KAlSi_3O_{8(adularia)} + 2CO_2 + 2H_2O; \quad (8)$$

and

$$HCO_3{}^- + H^- = CO + H_2O. \quad (9)$$

Silica flooding filling pore spaces and fractures at the auriferous No. 1-I Vein is characterized by abundant gas-rich and fluid-rich inclusions with identical temperatures and salinities of 0.7–6.7 wt.% NaCl. The silica is hosted by faults and tectonic breccia and where quartz veins and stockworks are also present with grades of up to 1200 ppm Au at the No. 1-I Vein, containing miarolitic, colloform and crustification textures at shallow depths. These features are characteristic of boiling fluids migrating along faults.

Given the ca. 99 Ma age of the mineralization and andesitic host rocks, and gold being deposited at relatively low temperatures of <300 °C, it is proposed that the gold has a magmatic source and deposited at shallow depths forming epithermal deposits. In addition, saccharoidal quartz at the No. 1-I Vein contains well-developed crystal-form quartz that is rich in primitive fluid inclusions with negative crystal form. This quartz contains thread- and flake-form gold in intergranular quartz pores (Fig. 5). These characteristics suggest that the mineralization has formed in a quiescent environment at structurally prepared sites (Figs. 16 and 18). The pattern of Au precipitation and enrichment is similar to that at the Porgera gold deposit in Papua New Guinea, where andesitic tectonic breccia containing plagioclase crystals that are up to 20 mm in diameter, and abundant fractures and air-holes and amygdaloidal textures that are up to 230 mm in diameter (Handley and Henry, 1990). These rocks with high-porosity can act as pathways carrying mineralized fluids to structural sites of deposition, such as tectonic breccia and faults, as is the case at Gaosongshan.

6.4. Gold in the Lesser Hinggan Range gold concentration area

The Lesser Hinggan Range belt is located along the margin of the Mesozoic volcanic Sunwu and Jiayin basins. Gold is located in the extensional faults at the margins of the basins, which are syn-depositional structures that have controlled sedimentation in the basins (Fig. 2; Liang et al., 2012).

The NW-trend of the Lesser Hinggan Range and the volcanic Songliao and Sunwu–Jiayin basins are controlled by region-wide extensional faults, such as the NW-trending Taxi–Linkou and Shagihe faults, and the NE-trending Wulaga Fault (Fig. 3a). These extensional faults and splays off them host granites and act as conduits for the mineralizing fluids.

Epithermal gold deposits are widespread in China in eastern China and were deposited from ca. 175 to 94 Ma, with the peak of mineralization between ca. 105 and 94 Ma, which are related to the interaction of the NCC with the Central Asia Orogen to the north, Qinlin Orogen to the south and the Paleo-Pacific Plate to the east (Fig. 1; Shao et al., 2001; Qi et al., 2005; Wang et al., 2006; Mao et al., 2007; Zhou et al., 2009b; Z.C. Zhang et al., 2010; J.H. Zhang et al., 2010; Wu et al., 2011; Zhen et al., 2012; Xu et al., 2013).

In the present Central Asian Orogen, Mesozoic subduction of the Mongol-Okhotsk Ocean (Van der Voo et al., 1999; Fan et al., 2003; Meng, 2003) beneath the Siberian Craton to the north subducted northward (Van der Voo et al., 1999; Fan et al., 2003; Meng, 2003). Whereas, the Paleo-Pacific Plate was accompanied by volcanism in NE China, which migrated from west to east during the Late Mesozoic without doming of the lithosphere (Xu et al., 2004; Wang et al., 2006; Zhou et al., 2009b; Zhang et al., 2006; J.H. Zhang et al., 2010).

Accretion of Jurassic terranes is widely distributed along the eastern Asian continental margin, including Northeast and Far East Russia, NE China and the Japanese Islands (Wu et al., 2011), which are associated

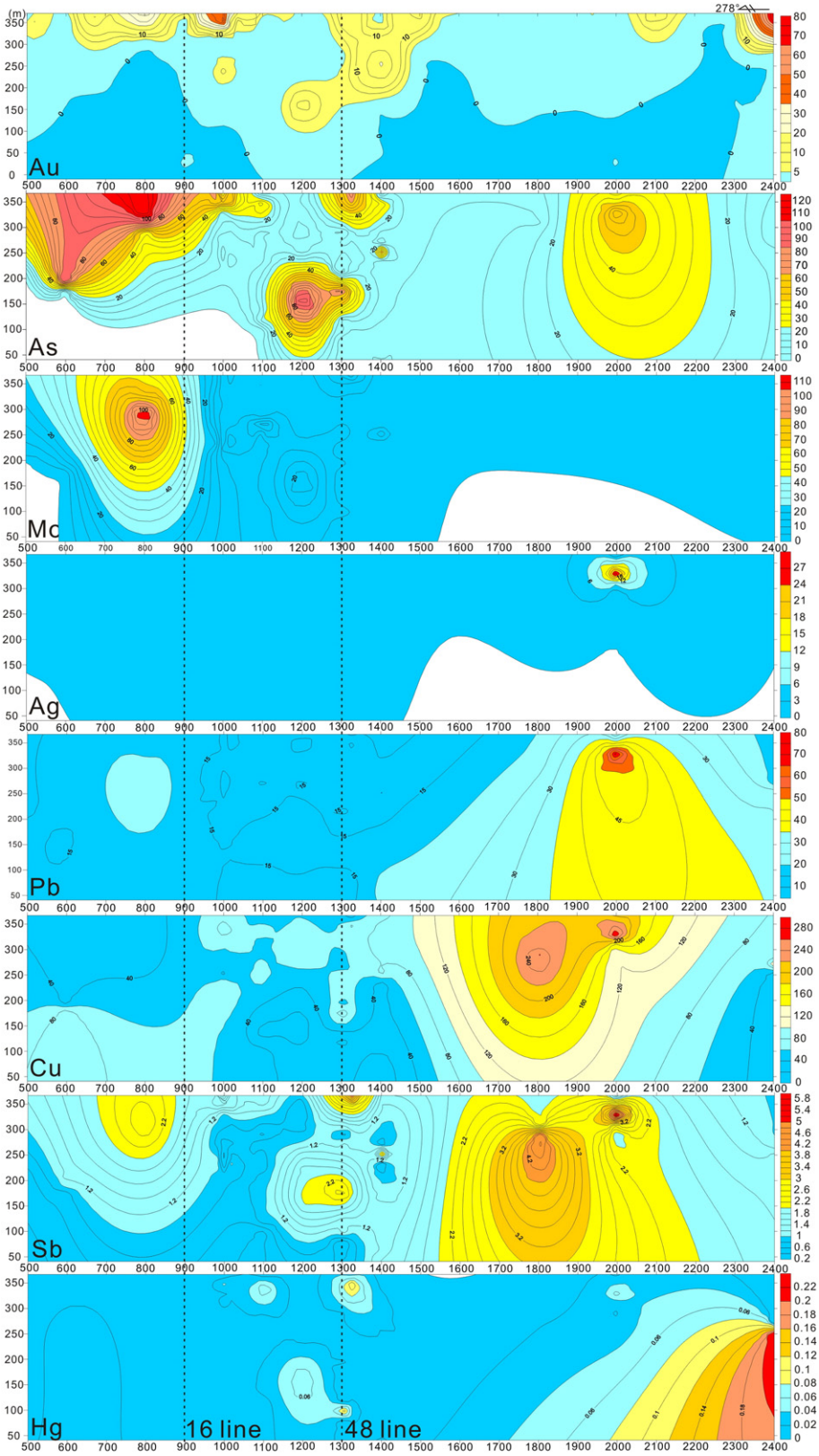

Fig. 16. Diagram showing equal values of element content from a longitudinal section of the No. I-1 vein in the Gaosongshan gold deposit.

with the subduction of the Paleo-Pacific plate between eastern China including the eastern Large Xinggan Range and Jilin–Heilongjiang provinces and the Jiaodong Peninsula (Zhou et al., 2009b; Wu et al., 2011; Zhang et al., 2012; Xu et al., 2013; Deng et al., 2014a, 2014b). These areas also contain gold deposits that are synchronous with the ca. 99 Ma Gaosongshan deposit. For example, the volcanic rocks assigned to the Early Cretaceous (ca. 115–111 Ma) Yingcheng Formation are intruded by post-orogenic A-type granites formed in an intracontinental extensional tectonic setting (Li et al., 2004; Zhang et al., 2007; Shu et al., 2007; Song et al., 2010). In NE China, the Early

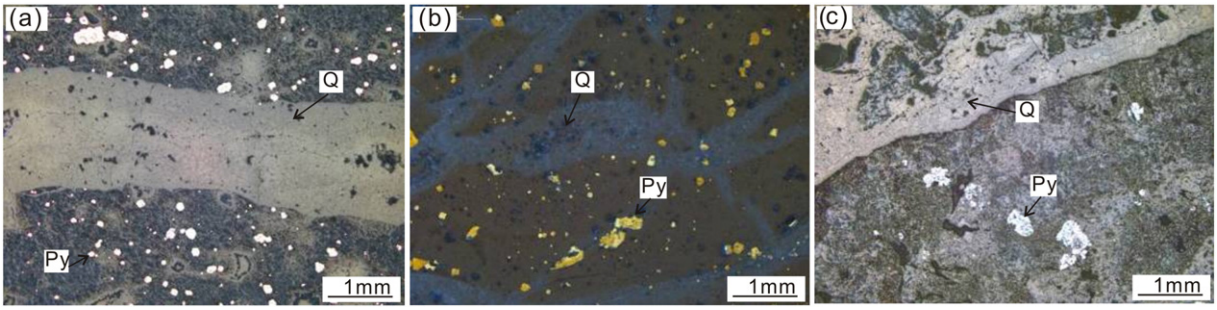

Fig. 17. Distribution of pyrite at the Gaosongshan gold deposit. Pyrite (Py) is distributed in altered andesitic breccia in samples: (a) GB1-1; (b) GB137-1; and (c) GM2-1.

Cretaceous (ca. 102 Ma) andesite units assigned to the Ganhe Formation at Dongan and the Banzifang Formation at Gaosongshan, which are widespread in the volcanic Sunwu and Jiayin basins, were formed in an active continental margin and arc setting (Z.C. Zhang et al., 2010; Hao, 2013). Rhyolite units that have A-type granitic geochemical signatures which were deposited ca. 97 Ma have an extensional tectonic setting (Hao, 2013). The volcanic rocks in the Fault-bound volcanic Sunwu and Jiayin basins have characteristics of intra-plate and convergent plate margin with the volcanism formed in a rift setting developed on the continental side of an active continental margin (Liang et al., 2012; Hao, 2013). Porphyritic granodiorite located to the west of the uplifted Jiamusi Massif formed in the transitional setting of the arc to the continent during ca. 114–80 Ma. It has been proposed that the gold mineralization in NE China was deposited in a magmatic-arc setting resulting from the NW-trending subduction of the Paleo-Pacific Plate during 125–110 Ma and 100–80 Ma (Koppers et al., 2001; Sato et al., 2002; Sun et al., 2009; Zhou et al., 2009b; Zhao et al., 2012; Xu et al., 2013).

Gold deposits distributed in the study region in the Lesser Hinggan Range, including, the 125–116 Ma Sandaowanzi deposit in the west (Liu et al., 2011), ca. 107 Ma Dongan deposit (Z.C. Zhang et al., 2010), ca. 99 Ma Gaosongshan deposit, and ca. 114–80 Ma Tuanjiegou deposit in the east (decrease in age from west to east). This systematic change in the age of the mineralization is related to the gradual eastward retreat of the subduction of the Paleo-Pacific Plate (Zhou et al., 2009b; J.H. Zhang et al., 2010; Hao, 2013).

6.5. Metallogenetic model

Magma chambers developed at depth during the subduction of the Paleo-Pacific Plate were the source of andesitic units assigned to the Early Cretaceous Banzifang Formation (Fig. 19). With the eastward retreat of the plate, the tectonic setting in the study area around Gaosongshan evolved from subduction to a back-arc extensional setting with the development of the fault-bound volcanic Sunwu and Jiayin basins west of the Jiamusi Massif. The volcanism progressed from the eruption of andesitic units in the Banzifang Formation to rhyolitic units in the Ningyuancun Formation. During the waning stage of the intermediate volcanism, mineralized fluid containing gold in solution formed through the interaction between the andesitic magma and late Paleozoic (260–253 Ma) crystalline crystal basement. The primary source of the gold is probably the lithospheric mantle, as deduced from the lead and sulfur isotope values determined from pyrite associated with gold. Driven by magmatic heat at depth, reduced mineralizing fluids migrated for a long distance along the Shaqihe Fault where it mixed meteoric water. Andesitic units associated with the early stage of the magmatism are the wall rocks to the mineralizing fluid. Gold was deposited from the fluid following fluctuations in pressure during ca. 99 Ma throughout the Lesser Hinggan Range.

7. Conclusions

Gaosongshan in NE China is a low-sulfidation epithermal Au deposit characterized by the assemblage quartz–adularia–sericite. The mineralization was deposited at low temperatures from a fluid with low salinity during ca. 99 Ma in the early Cretaceous.

The sulfur and lead isotope studies suggest that pyrite associated with gold mineralization at Gaosongshan is partly derived from the lithospheric mantle with contributions from the lower crust.

The ore-forming fluids have a meteoric source containing minor gaseous phases, which is a composition that played a critical role in the transportation and precipitation of gold. The gold was precipitated with reductions in fluid pressures during boiling, which was probably due to drops in pressure during movement along the host structures.

The deposition of epithermal gold mineralization throughout the Lesser Hinggan Range appears to be uniform and controlled by movements along extensional fault controlling the deposition of volcanic successions in a back-arc basin developed in an active continental margin. Finally, the gold mineralization in the basin has a similar genesis to that of the porphyry Au (–Cu) deposits associated with the subduction

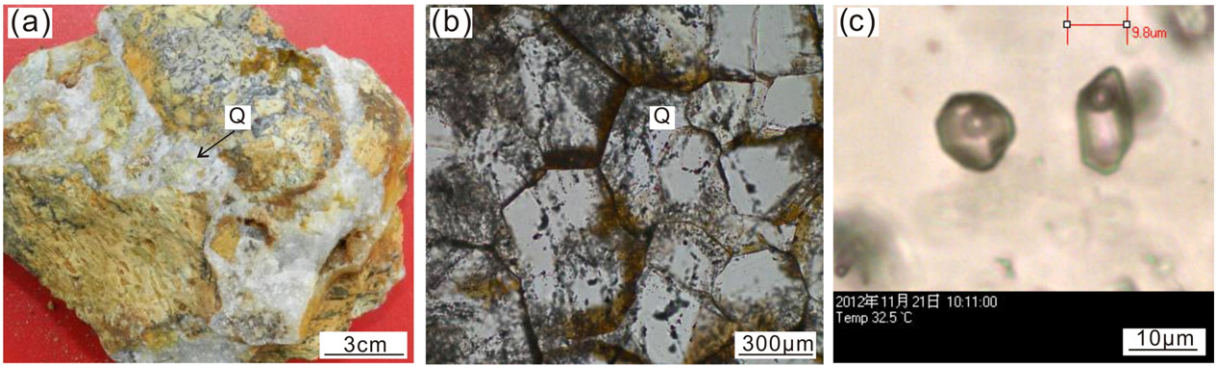

Fig. 18. Sucrose quartz and its internal structure with primary fluid inclusions at the Gaosongshan gold deposit (Sample GB-1-69): (a) breccia-type ore, with quartz (Q) flooding acting as a cement; (b) quartz with well-developed crystal form; and (c) fluid inclusions with primitive negative crystal form.

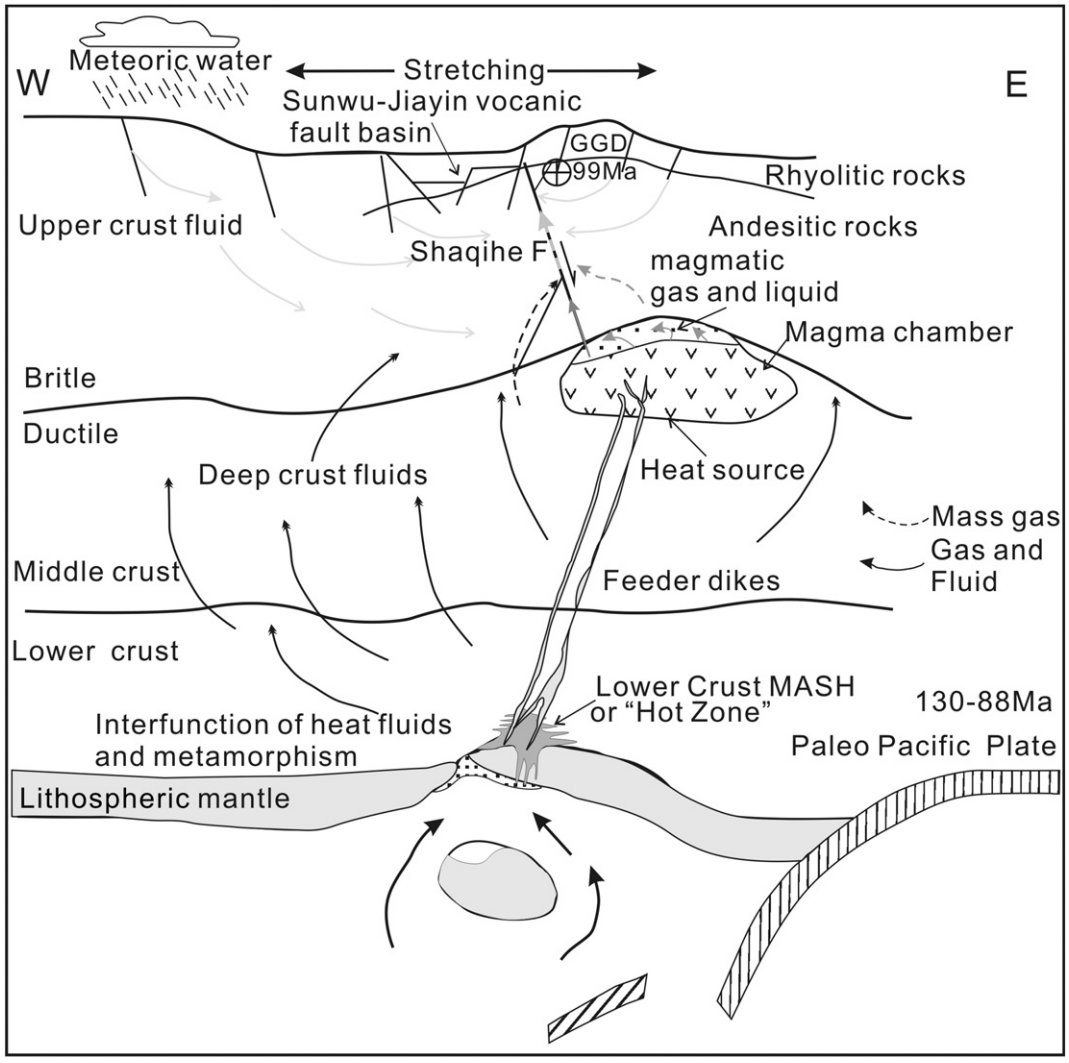

Fig. 19. Metallogenetic model for the Gaosongshan gold deposit (GGD).

of the Paleo-Pacific plate along the margin of the eastern Jilin and Heilongjiang provinces of China.

Acknowledgments

We thank our colleagues for their great support during the geological and gold deposit investigations at the Gaosongshan mine and for their assistance in geochemical and isotope analyses. We are also grateful to Professors Gu X.X. and Liang Y.H. for reference to their unpublished data, and researchers Drs Hou Z.Q. and Chen Y.J. for their constructive reviews and suggestions. Drs Jiang S.H., Fei H.C., and two anonymous referees are thanked for their thoughtful, constructive comments, and editorial refinements.

References

Bian, H.Y., Chen, M., Liu, H.L., Zhao, C.R., 2009. Geology and genesis of the Gaosongshan gold deposit in Xunke Country, Heilongjiang province. Geol. Resour. 8, 91–95 (in Chinese with English abstract).

Brown, K.B., 1986. Gold deposition from geothermal discharges in New Zealand. Econ. Geol. 81, 979–983.

Chen, G.W., Xia, B., Xiao, Z.Y., Yu, H.X., Wang, H., Zhong, Z.H., Wang, G.Q., 2001. Characteristics of epithermal deposits and the prospecting guide in China. Geol. Resour. 10, 165–171 (in Chinese with English abstract).

Chen, Y.J., Zhang, C., Li, N., Yang, Y.F., Deng, K., 2012. Geology of the Mo deposits in Northeast China. J. Jilin Univ. (Earth Sci. Educ.) 42, 1224–1268 (in Chinese with English abstract).

Ciobanu, C.L., Cook, N.J., Pring, A., Brugger, J., Danyushevsky, L.V., Shimizu, M., 2009. 'Invisible gold' in bismuth chalcogenides. Acta Geochim. Cosmochim. 73, 1970–1999.

Cooke, D.R., Simmons, S.F., 2000. Characteristics and genesis of epithermal gold deposits. Soc. Econ. Geol. Rev. Econ. Geol. 13, 163–220.

Corbett, G., 2002. Epithermal gold for explorationists. AIG J. Appl. Geosci. Pract. Res. Aust. 1, 1–26.

Deng, J., Yuan, W.M., Carranza, E.J.M., Yang, L.Q., Wang, C.M., Yang, L.Y., Hao, N.N., 2014a. Geochronology and thermochronometry of the Jiapigou gold belt, northeastern China: new evidence for multiple episodes of mineralization. J. Asian Earth Sci. 89, 10–27.

Deng, J., Liu, X.F., Wang, Q.F., Pan, R.G., 2014b. Origin of the Jiaodong-type Xinli gold deposit, Jiaodong Peninsula, China: constraints from fluid inclusion and C–D–O–S–Sr isotope compositions. Ore Geol. Rev. http://dx.doi.org/10.1016/j.oregeorev.2014.04.018.

Doe, B.R., Zartman, R.E., 1979. Plumbotectonics, the Phanerozoic. In: Barnes, H.L. (Ed.), Geochemistry of Hydrothermal Ore Deposits, 2nd edition John Wiley & Sons Inc., pp. 2–70.

Einaudi, M.T., Hedenquist, J.W., Inan, E., 2003. Sulfidation state of fluids in active and extinct hydrothermal system: transitions from porphyry to epithermal environments. Soc. Econ. Geol. Spec. Publ. 10, 28–314.

Fan, W.M., Guo, F., Wang, Y.J., Lin, G., 2003. Late Mesozoic calc-alkaline volcanism of post-orogenic extension in the northern Da Hinggan Mountains, northeastern China. J. Volcanol. Geotherm. Res. 121, 115–135.

Giggenbach, W.F., 2003. Magma degassing and mineral deposition in hydrothermal systems along convergent plate boundaries. Soc. Econ. Geol. Spec. Publ. 10, 1–18.

Guo, J.H., Wang, C.S., Shi, Y.J., 2004. Geological and geochemical features of the Dong'an gold deposit in Heilongjiang. Geol. Explor. 40, 37–41 (in Chinese with English abstract).

Han, S.Y., Zhai, D.G., Liu, J.J., Lu, J., Wu, S.H., Yang, L.B., 2011. Mineral assemblage of Sandaowanzi tellurium–gold deposit in Heilongjiang Province and its genetic significance. Mineral Deposits 30, 855–866 (in Chinese with English abstract).
Handley, G.A., Henry, D.D., 1990. Porgera gold deposit. In: Hughes, F.E. (Ed.), Geology of the Mineral Deposits of Australia and Papua New Guinea. Aust. Inst. Min. Metall. Monogr 14, pp. 1717–1724.
Hao, B.W., 2012. Discovering of the adakites and genesis and U–Pb ages of the zircons and tectonic significance about the granites in Narenwula of Inner Mongolia. J. Mineral. Petrol. 32, 28–39 (in Chinese with English abstract).
Hao, B.W., 2013. Mesozoic Tectonic and Magmatic Evolution and Gold Metallogenic Study of the Northern Lesser Xinggan Range. (Postdoctoral Thesis), China University of Geosciences, Beijing (186 pp. in Chinese).
Hao, B.W., Hou, Z.Q., 2012. Discovery of the Early Paleozoic Bainaimiao-Odor Sum Island Arc in the Hadamiao Gold Ore district, Inner Mongolia and its significance to the evolution of the Paleo-Asian Ocean. Acta Geol. Sin. 86, 801–840 (in Chinese with English abstract).
He, X.X., Zhu, X.K., Yang, C., Tang, S.H., 2005. High-precision analysis of Pb isotope ratios using MC-ICP-MS. Acta Geosci. Sin. 26, 19–22 (in Chinese with English abstract).
Hedenquist, J.W., Lowenstern, J.B., 1994. The role of magmas in the formation of hydrothermal ore deposits. Nature 370, 519–527.
Hedenquist, J.W., Arribas, R.A., Gonzalez, U.E., 2000. Exploration for epithermal gold deposits. Rev. Econ. Geol. 13, 245–277.
Heinrich, C.A., Ryan, G.G., Mernagh, T.P., Eadington, P.J., 1992. Segregation of ore metals between magmatic brine and vapor: a fluid inclusion study using PIXE microanalysis. Econ. Geol. 87, 1566–1583.
Heinrich, C.A., Driesner, T., Stefansson, A., Seward, T.M., 2004. Magmatic vapor contraction and the transport of gold from the porphyry environment to epithermal ore deposits. Geology 32, 761–764.
Henley, R.W., 1990. Ore transport and deposition in epithermal environments. In: Herbert, H.K., Ho, S. (Eds.), Stable Isotope and Fluid Processes in Mineralization. Geology Department and University Extension. The University of Western Australia, pp. 51–89 (Publication 23).
Hoefs, J., 2009. Stable Isotope Geochemistry. 6th edition. Springer-Verlag, Berlin Heidelberg (285 pp.).
Hou, K.J., Li, Y.H., Tian, Y.Y., 2009. In situ U–Pb zircon dating using laser ablation-multi ion counting-ICP-MS. Mineral. Deposita 28, 481–492 (in Chinese with English abstract).
Jiang, S.H., Nie, F.J., Zhang, Y., Hu, P., 2004. The latest advances in the research of epithermal deposits. Earth Sci. Front. 11, 401–411 (in Chinese with English abstract).
Koppers, A.P., Morgan, J.P., Morgan, J.W., Staudigel, H., 2001. Testing the fixed hotspot hypothesis using $^{40}Ar/^{39}Ar$ age progressions along seamount trails. Earth Planet. Sci. Lett. 185, 237–252.
Li, B.L., Wang, J., 1998. The relation between granitic porphyry mass and gold mineralization of Tuanjiegou gold deposit, Heilongjiang Province. Gold 19, 3–6 (in Chinese with English abstract).
Li, J.Y., Mo, S.G., He, Z.J., Sun, G.H., Chen, W., 2004. The timing of crustal sinistral strike-slip movement in the northern Great Khingan ranges and its constraint on reconstruction of the crustal tectonic evolution of NE China and adjacent areas since the Mesozoic. Earth Sci. Front. 11, 157–168 (in Chinese with English abstract).
Li, J.Q., Zhou, K., Jin, T.H., 2008. Geological characters and origin of Tuangjiegou gold deposit, Heilongjiang Province. Gold 6, 19–24 (in Chinese with English abstract).
Lian, Y.L., Wang, X.C., 2010. The metallogenetic rules and exploitation targets. Met. Miner. 408, 119–122 (in Chinese with English abstract).
Liang, Y.H., Zhang, H.Y., Liu, X.S., Qi, Y., Feng, J., Li, M., 2012. The study of the rules of ores controlled by structures in the Gaosongshan gold deposit, Xunke country, Heilongjiang Province. Jilin University Unpublished Item Report.
Lindgren, W., 1922. A suggestion for a terminology of certain mineral deposits. Econ. Geol. 17, 292–294.
Lindgren, W., 1933. Mineral Deposits. 4th ed. McGraw-Hill, New York (930 pp.).
Liu, G.G., Wang, E.D., Chang, C.J., Jin, B.Y., Yu, W.Q., 2006. Discussion on metallogeny of Gaosongshan Gold Deposit, Xunke Country, Heilongjiang Province. Nonferrous Min. Metall. 22, 1–4 (in Chinese with English abstract).
Liu, J.F., Chi, X.G., Dong, C.Y., Zhao, Z., Li, G.R., Zhao, Y.D., 2008. Discovery of Early Paleozoic granites in the eastern Lesser Xinggan Range, northeastern China and their tectonic significance. Geol. Bull. China 27, 534–544 (in Chinese with English abstract).
Liu, Y.S., Gao, S., Hu, Z.C., Gao, C.G., Zong, K.Q., Wang, D.B., 2010. Continental and oceanic crust recycling-induced melt-peridotite interactions in the Trans-North China Orogen: U–Pb dating, Hf isotopes and trace elements in zircons from mantle xenoliths. J. Petrol. 51, 537–571.
Liu, J.L., Bai, X.D., Zhao, S.J., Tran, M.D., Zhang, Z.C., Zhao, Z.D., Zhao, H.B., Lu, J., 2011. Geology of the Sandaowanzi telluride gold deposit of the northern Great Xingan Range, NE China: geochronology and tectonic controls. J. Asian Earth Sci. 41, 107–118.
Ludwig, K.R., 2003. ISOPLOT 3.00: A Geochronological Toolkit for Microsoft Excel. Berkeley Geochronology Center (Special Publication No. 4).
Mao, J.W., Li, X.F., White, N.C., Zhao, C.S., Zhang, Z.H., Wang, Y.T., Hu, H.B., 2007. Types, characteristics, and geodynamic settings of Mesozoic epithermal gold deposits in Eastern China. Resour. Geol. 57, 435–454.
Matsuhisa, Y., Goldsmith, J.R., Clayton, R.N., 1979. Oxygen isotope fractionation in the system quartz–albite–anorthite–water. Geochim. Cosmochim. Acta 43, 1131–1140.
Meng, Q.R., 2003. What drove late Mesozoic extension of the northern China–Mongolia tract? Tectonophysics 369, 155–174.
Nasdala, L., Hofmeister, W., Norberg, N., Mattinson, J.M., Corfu, F.D., Kamo, S.L., Kennedy, A.K., Kronz, A., Reiners, P.W., Frei, D., Kosler, J., Wan, Y., Gtze, J., Hger, T., Krner, A., Valley, J., 2008. Zircon M257—a homogeneous natural reference material for the ion microprobe U–Pb analysis of zircon. Geostand. Newslett. 32, 247–265.
Pudack, C., Halter, W.E., Heinrich, C.A., Pettke, T., 2009. Evolution of magmatic vapor to gold-rich epithermal liquid: the porphyry to epithermal transition at Nevados de Famatina, northwest Argentina. Econ. Geol. 104, 449–477.
Qi, J.P., Chen, Y.J., Pirajno, F., 2005. Geological characteristics and tectonic setting of the epithermal deposits in the northeast China. J. Mineral. Petrol. 25, 47–59 (in Chinese with English abstract).
Richards, J.P., 2011. Magmatic to hydrothermal metal fluxes in convergent and collided margins. Ore Geol. Rev. 40, 1–26.
Robb, L., 2005. Introduction to Ore-forming Processes. Blackwell Publishing, U.K. (373 pp.).
Rowland, J.V., Simmons, S.F., 2012. Hydrologic magmatic, and tectonic controls on hydrothermal flow, Taupo Volcanic Zone, New Zealand: implications for the formation of epithermal vein deposits. Econ. Geol. 107, 427–457.
Sato, K., Vrublevsky, A.A., Rodionov, S.M., Pomanovsky, N.P., Nedachi, M., 2002. Mid-Cretaceous episodic magmatism and tin mineralization in Khingan–Okhotsk volcanic–plutonic belt. Far East Russ. Resour. Geol. 52, 1–14.
Seo, J.H., Guillong, M., Heinrich, C.A., 2009. The role of sulfur in the formation of magmatic–hydrothermal copper–gold deposits. Earth Planet. Sci. Lett. 282, 323–328.
Shao, J.A., Liu, F.T., Chen, H., Han, Q.J., 2001. Relationship between Mesozoic magmatism and subduction in Da Hinggan–Yanshan area. Acta Geol. Sin. 75, 56–63.
Shao, J.A., Mu, B.L., Zhu, H.Z., Zhang, L.Q., 2010. Material source and tectonic sitting of the Mesozoic mineralization of the Da Hinggan Mts. Acta Petrol. 26, 649–656 (in Chinese with English abstract).
Shen, W.Z., 1997. Stable Isotopic Geology Tutorial. Atomic Energy Publishing House, Beijing (287 pp., in Chinese).
Shu, P., Ding, R.X., Ji, X.Y., Qu, Y.M., 2007. SHRIMP zircon geochronology of reservoir volcanic rocks in the Qingshen gas field, Songliao Basin. Acta Petrol. Mineral. 32, 15–20 (in Chinese with English abstract).
Sillitoe, R.H., 1993. Epithermal models: genetic types, geometrical controls and shallow features. Geol. Assoc. Can. Spec. Pap. 40, 403–417.
Sillitoe, R.H., 2000. Gold-rich porphyry deposits: descriptive and genetic models and their role in exploration and discovery. Rev. Econ. Geol. 13, 315–345.
Sillitoe, R.H., Hedenquist, J.W., 2003. Linkages between volcanotectonic settings, ore fluid compositions, and epithermal precious metal deposits. Soc. Econ. Geol. Spec. Publ. 10, 315–343.
Simmons, S.F., Browne, P.R.L., 2000. Hydrothermal minerals and precious metals in the Broadlands–Ohaaki geothermal system: implications for understanding low-sulfidation epithermal environments. Econ. Geol. 95, 971–999.
Simmons, S.F., White, N.C., John, D.A., 2005. Geological characteristics of epithermal precious and base metal deposits. Economic Geology 100th Anniversary Volumepp. 485–522.
Song, L.Z., Zhao, Z.H., Jiao, G.H., Sun, P., Luo, X., Jiang, X.H., Wang, Z.H., Zeng, F.Y., Liao, W.D., 2010. Geochemical characteristics of Early Cretaceous volcanic rocks from Songliao Basin, Northeast China, and its tectonic implications. Acta Pet. Sin. 26, 1182–1194 (in Chinese with English abstract).
Sun, D.Y., Wu, F.Y., Gao, S., Lu, X.P., 2005. Confirmation of two episodes A-type granite emplacement during Late Triassic and Early Jurassic in the central Jilin Province, and their constraints on the structural pattern of Jilin–Heilongjiang Area, China. Earth Sci. Front. 12, 263–275 (in Chinese with English abstract).
Sun, F.Y., Wang, L., Huo, L., Wang, K.Y., 2008. Fluid inclusions study on Wulaga gold deposit in Heilongjiang Province and implications for ore genesis. Geol. China 35, 1267–1273 (in Chinese with English abstract).
Sun, J.G., Men, L.J., Chen, D., Chen, L., Pang, W., Liang, S.N., Chang, Y., Nie, X.T., 2009. Constraints of magmatism of the ore-forming process of magmatic hydrothermal gold-rich copper deposits as recorded from the element geochemistry and zircon CL image features: a case study of the Xiaoxinancha gold-rich copper deposit, Yangbian, Jilin province. J. Mineral. Petrol. 29, 44–52 (in Chinese with English abstract).
Tang, Z., Ye, S.Q., Yang, Y.C., 2010. Discussion on metallogenic model of Gaoshongshan gold deposit in Xunke of Heilongjiang. Glob. Geol. 29, 399–407 (in Chinese with English abstract).
Taylor, S.R., McLennan, S.M., 1985. The Continental Crust: Its Composition and Evolution. Blackwell Scientific Publishers, Oxford (312 pp.).
Van der Voo, R., Spakman, W., Bijwaard, H., 1999. Mesozoic subducted slabs under Siberia. Nature 397, 246–249.
Wang, K.Y., Ren, Y.S., Cheng, X.M., Dai, J.Z., 2004. Study on fluid inclusions of Tuanjiegou Gold deposit in Heilongjiang Province and implication for its genesis. Geotecton. Metallog. 28, 171–178 (in Chinese with English abstract).
Wang, F., Zhou, X.H., Zhang, L.C., Ying, J.F., Zhang, Y.T., Wu, F.Y., Zhu, R.X., 2006. Late Mesozoic volcanism in the Great Xing'an Range (NE China): timing and implications for the dynamic setting of NE Asia. Earth Planet. Sci. Lett. 251, 179–198.
Wang, Y.B., Liu, J.M., Sun, S.K., Li, Y., Li, F.Y., Hu, H.T., 2012. Zircon U–Pb geochronology, petrogenesis and geological implication of ore-bearing granodiorite porphyry in the Wulaga gold deposit, Heilongjiang Province. Acta Pet. Sin. 28, 557–570 (in Chinese with English abstract).
Wilde, S.A., Wu, F.Y., Zhao, G.C., 2010. The Khanka Block, NE China, and its significance for the evolution of the Central Asian Orogenic Belt and continental accretion. Geol. Soc. Lond. Spec. Publ. 338, 117–137.
Wu, F.Y., Sun, D.Y., Ge, W.C., Zhang, Y.B., Grant, M.L., Wilde, S.A., Jahn, B.M., 2011. Geochronology of the Phanerozoic granitoids in northeastern China. J. Asian Earth Sci. 41, 1–30.
Xiao, W.J., Windley, B.F., Hao, J., Zhai, M.G., 2003. Accretion leading to collision and the Permian Solonker suture, Inner Mongolia, China: termination of the central Asian orogenic belt. Tectonics 22, 1189–1217.
Xu, Y., He, B., Chung, S.L., Menzies, M.A., Frey, F.A., 2004. Geologic, geochemical, and geophysical consequences of plume involvement in the Emeishan flood-basalt province. Geology 32, 917–920.
Xu, J.H., Wei, H., Wang, Y.H., Zeng, Q.D., Liu, J.M., Wang, Y.B., Mao, Q., 2012. Sub-volcanic hydrothermal mineralization of the Wulaga gold deposit, Heilongjiang, China: evidences from melt and fluid inclusions. Acta Petrol. Sin. 28, 1305–1316 (in Chinese with English abstract).

Xu, W.L., Wang, F., Pei, F.P., Meng, E., Tang, J., Xu, M.J., Wang, W., 2013. Mesozoic tectonic regimes and regional ore-forming background in NE China: constraints from spatial and temporal variations of Mesozoic rock associations. Acta Petrol. Sin. 29, 339–353 (in Chinese with English abstract).

Zartman, R.E., Doe, B.R., 1981. Plumbotectonics—the model. In: Zartman, R.E., Taylor, S.R. (Eds.), Evolution of the Upper Mantle. Tectonophysics 75, pp. 135–162.

Zhai, D.G., Lui, J.J., Han, S.Y., Wang, J.P., Zhang, H.Y., Liu, Z.J., 2013. Typomorpic characteristics of pyrite and processes of changes and preservation of the Sandaowanzi telluride–gold deposit in Heilongjiang Province. Acta Petrol. Sin. 87, 81–90 (in Chinese with English abstract).

Zhang, L.G., Zhuang, L.C., Qian, Y.O., Guo, Y.S., Zhe, P., 1981. Stable isotope geochemistry of granite and W, Sn deposit in Xihuashan Piaotang, Jiangxi Province. Proceedings of the Symposium on Tungsten Geology. Geological Publishing House, Beijing, pp. 325–338 (in Chinese).

Zhang, Z.C., Mahoney, J.J., Mao, J.W., Wang, F.S., 2006. Geochemistry of picritic and associated basalt flows of the western Emeishan flood basalt province, China. J. Petrol. 47, 1997–2019.

Zhang, F.Q., Pang, Y.M., Yang, S.F., Dong, C.W., Chen, H.L., Shu, P., 2007. Geochronology of zircon SHRIMP geochemistry and its implication of the volcanic rocks from Yingcheng Formation in depression area, North of Songliao basin. Acta Geol. Sin. 81, 1248–1258 (in Chinese with English abstract).

Zhang, Z.C., Mao, J.W., Wang, Y.B., Pirajno, F., Liu, J.L., Zhao, Z.D., 2010. Geochemistry and geochronology of the volcanic rocks associated with the Dong'an adularia–sericite epithermal gold deposit, Lesser Hinggan Range, Heilongjiang province, NE China: constraints on the metallogenesis. Ore Geol. Rev. 37, 158–174.

Zhang, J.H., Gao, S., Ge, W.C., Wu, F.Y., Yang, J.H., Wilde, S.A., Li, M., 2010. Geochronology of the Mesozoic volcanic rocks in the Great Xing'an Range, northeastern China: implications for subduction induced delamination. Chem. Geol. 276, 144–165.

Zhang, X.Z., Ma, Y.X., Chi, X.G., Zhang, F.X., Sun, Y.W., Guo, Y., Zeng, Z., 2012. Discussion on Phanerozoic tectonic evolution in northeastern China. J. Jilin Univ. 42, 1269–1285.

Zhao, H.H., Xue, J.G., Li, X.D., Huang, W., 2011. The characters and prospecting of ore-controlling structures in Gaosongshan Gold Deposit. Sci. Technol. West. China 10, 14–16 (in Chinese with English abstract).

Zhao, Y.S., Yang, L.Q., Chen, Y.F., Qing, M., Yan, J.P., Ge, L.S., Guo, X.D., Wang, J.R., 2012. Geochemistry and zircon U–Pb geochronology of the diorite porphyry associated with the Jinchang Cu–Au deposit, Heilongjiang Province. Acta Petrol. Sin. 28, 451–467 (in Chinese with English abstract).

Zhen, Y.Q., Niu, S.Y., Diao, Q., Ye, L.W., Wu, J., Song, T., Jia, X.Y., 2012. The mantle plume structure and mineralization effect in Northeast China. Acta Geol. Sin. 86, 1869–1889 (in Chinese with English abstract).

Zhou, J.B., Wilde, S.A., Zhang, X.Z., Zhao, G.C., Zheng, C.Q., Wang, Y.J., Zhang, X.H., 2009a. The onset of Pacific margin accretion in NE China: evidence from the Heilongjiang high-pressure metamorphic belt. Tectonophysics 478, 230–246.

Zhou, J.B., Zhang, X.Z., Ma, Z.H., Liu, L., Jin, W., Zhang, M.S., Wang, C.W., Chi, X.G., 2009b. Tectonic framework and basin evolution in Northeast China. Oil Gas Geol. 30, 530–538 (in Chinese with English abstract).

Zhou, J.B., Wilde, S.A., Zhao, G.C., Zhang, X.Z., Zheng, C.Q., Wang, H., Zeng, W.S., 2010. Pan-African metamorphic and magmatic rocks of the Khanka Massif, NE China: further evidence regarding their affinity. Geol. Mag. 147, 737–749.